Seasonal simulations over North America with a GCM and three regional models

E. Altshuler, M. Fennessy, and J. Shukla

Center for Ocean-Land-Atmosphere Studies, Calverton, MD

H. Juang, E. Rogers, and K. Mitchell

Environmental Modeling Center, National Centers for Environmental Prediction, Washington, DC

M. Kanamitsu

Scripps Institution of Oceanography, La Jolla, CA

March 2002

Abstract

Seasonal hindcasts have been carried out using the Center for Ocean-Land-Atmosphere Studies (COLA) R40 atmospheric general circulation model and 80-km resolution versions of three regional models: the National Centers for Environmental Prediction (NCEP) Eta model, the NCEP Regional Spectral Model (RSM), and two versions of the Pennsylvania State University (PSU)/National Center for Atmospheric Research (NCAR) MM5 mesoscale model. Simulations for three summer and three winter seasons have been performed over the North American region. The COLA GCM was initialized using observed atmospheric analyses, while each of the regional models was provided with initial and lateral boundary conditions from NCEP/NCAR reanalysis data. All of the models used observed global sea surface temperature (SST) which was prescribed and updated throughout the integrations. Initial land surface conditions varied among the models but were kept as consistent as possible.

Examination of the ensemble seasonal mean simulations shows that all of the regional models, except RSM, demonstrate greater skill than the GCM in simulating seasonal mean precipitation for both summer and winter. The RSM simulations contain a large systematic moist bias in both seasons. For seasonal mean surface temperature, RSM is clearly superior to the other models, especially in winter. RSM, and to a lesser extent the Eta model, provide the best simulation of the summer 850-mb circulation, particularly the low-level jet (LLJ) over the U.S. southern plains.

The models' ability to simulate interannual variability was assessed by examining the simulated summer 1993 (excessively wet) versus 1988 (drought conditions) climate features over the central U.S. The overall results are rather disappointing, although the Eta and RSM do show some apparent skill in capturing the precipitation, surface temperature, and 850-mb circulation differences between the two years. The GCM and both versions of MM5 do not demonstrate any discernable skill in simulating this interannual variability.

The computational efficiency of the regional models has also been evaluated. Considering both model performance and efficiency, the Eta model appears most favorable among the models considered. RSM performs well in some respects but is computationally expensive, while neither version of MM5 appears to be competitive with the other models on the basis of either performance or efficiency.

1. Introduction

A body of recent research has shown that seasonal climate anomalies are forced in part by slowly varying boundary conditions of sea surface temperature (SST) and land surface conditions. The ability of coupled ocean-atmosphere models to predict tropical SST anomalies has been well established. Thus, it is possible that accurate predictions of surface boundary conditions could allow prediction of regional climate anomalies for lead times beyond the limit of deterministic predictability (Shukla 1998). However, current atmospheric general circulation models (AGCMs) do a poor job of simulating regional precipitation anomalies over the continents, even with prescribed observed global SST anomalies. It may be that current AGCMs do not have sufficient horizontal resolution to adequately resolve regional orographically forced precipitation features.

One approach to address this problem is to use a low-resolution coupled ocean-land-atmosphere model to predict the anomalous surface boundary conditions of SST, soil wetness and snow depth. The predicted boundary conditions can then be used by a medium-resolution global atmospheric model that is integrated for a season to produce the global circulation and planetary-scale waves that occur in response to the anomalous boundary conditions. A limited area high-resolution atmospheric model is then nested in the global atmospheric model by applying the global circulation predicted by the medium-resolution model as a lateral boundary condition to the high-resolution regional model. Given a sufficiently large domain for the nested model, this matching at the boundaries only specifies the continental scale heat and moisture flux divergences and allows the actual distribution of temperature and precipitation within the domain to be significantly different from that of

the global model. The regional climatic details that are indistinct or even erroneous in the medium-resolution model could be more skillfully predicted by the high-resolution model. This procedure allows us to address the following question: Can the predictable component of the large-scale circulation be used in conjunction with high-resolution regional dynamical models to predict regional climate in North America at seasonal and longer lead times? Results of Giorgi and Bates (1989) and Giorgi (1990) for the western U.S., Ji (1996) and Ji and Vernekar (1997) for the Indian monsoon region and of Tanajura (1996) for the South American region, among others, have already provided a strong scientific justification of this procedure. Most recently, Fennessy and Shukla (2000) have presented results of similar experiments for the North American region. In this paper, we adopt a slightly different strategy in that we use the observed large-scale circulation, rather than that obtained from a GCM, to drive the regional models. This procedure is sometimes referred to as a "perfect boundary conditions" experiment, since it eliminates errors associated with the GCM and theoretically should yield superior results in seasonal hindcast experiments. In our case, we have used data from the National Centers for Environmental Prediction (NCEP)/National Center for Atmospheric Research (NCAR) reanalysis project (Kalnay et al. 1996; Kistler et al. 2001; now referred to as Reanalysis-I) to approximate the observed large-scale fields.

We have performed seasonal hindcasts for three summers and three winters over the North American region using the COLA GCM and three regional models: the NCEP Environmental Modeling Center (EMC) Eta model (Black 1994), the Pennsylvania State University (PSU)/NCAR Mesoscale Model (MM5) (Dudhia 1993; Grell et al. 1994), and the NCEP Regional Spectral Model (RSM) (Juang and Kanamitsu 1994; Juang et al. 1997). The

integration domains (shown in Fig. 1) and horizontal resolutions of the regional models have been chosen to be as consistent as possible with each other. The Eta model was chosen following the successful results of Ji and Vernekar (1997) in simulating seasonal mean features and interannual variability of the Indian summer monsoon rainfall, Tanajura (1996) in simulating the South American climate, and Fennessy and Shukla (2000) in simulating seasonal mean features and interannual variability of the North American climate. We chose MM5 because it is a well-supported research model which, given suitable modifications, can be used in regional climate simulations [the model used by Giorgi and Bates (1989) and Giorgi (1990) is based on MM4, a predecessor of MM5]. Finally, we selected the RSM based on the successful results of Hong and Leetmaa (1999) in simulating regional climate over the U.S. and Hong et al. (1999) for the East Asian monsoon region.

The model formulations and experimental design are described in Sections 2 and 3, respectively. The seasonal mean climate hindcasts are presented in Section 4. Aspects of the simulation of the observed interannual variability are discussed in Section 5. A summary and conclusions are given in Section 6.

2. Description of the models

a. COLA GCM

The COLA GCM is based on a modified version of the National Centers for Environmental Prediction (NCEP) global spectral model used for medium range weather forecasting [see Sela (1980) for original NCEP formulation; see Kinter et al. (1988, 1997) and Dewitt (1996) for the modified version]. The land surface parameterization was changed

to the Simple Biosphere model (SiB) biophysical formulation after Sellers et al. (1986) by Sato et al. (1989) and later simplified by Xue et al. (1991). The model uses relaxed Arakawa-Schubert convection [Moorthi and Suarez 1992; after Arakawa and Schubert (1974)] and Tiedtke (1984) shallow convection after Hogan and Rosemond (1991), and is described by Dewitt (1996).

The COLA GCM is a global spectral model with rhomboidal truncation at zonal wave number 40 (R40). The model physics calculations are done on a 1.8° latitude by 2.8° longitude Gaussian grid. The vertical structure of the model is represented by 18 unevenly spaced levels using σ as the vertical coordinate (Phillips 1957). The spacing of the levels is such that greater resolution is obtained near the earth's surface and at the tropopause. In addition to the parameterizations mentioned above, the COLA GCM includes parameterizations of solar radiative heating (Lacis and Hansen 1974), terrestrial radiative heating (Harshvardhan et al. 1987), large scale condensation, cloud-radiation interaction [Hou 1990; after Slingo (1987)], gravity wave drag [Vernekar et al. 1992; after Alpert et al. (1988)] and a turbulence closure scheme for subgrid scale exchanges of heat, momentum and moisture (Miyakoda and Sirutis 1977; Mellor and Yamada 1982).

In the COLA GCM, each land grid box (approximately 1.8° latitude x 2.8° longitude) is assigned one of twelve sets of vegetation and soil characteristics, based on the dominant vegetation observed in the grid box (Dorman and Sellers 1989; Fennessy and Xue 1997). Included in these characteristics are the depth and porosity of each of three soil layers: the surface layer, the root zone and the drainage layer. The total depth of the three layers ranges from 49 cm for bare soil (desert) to 350 cm for trees. The total water holding

capacity ranges from 21 cm for bare soil to 147 cm for trees. The soil wetness is initialized from proxy seasonally varying soil wetness derived from data produced by the ECMWF analysis-forecast system (Fennessy and Shukla 1996). The model uses mean orography (shown in Fig. 2a) calculated from the U.S. Navy 10-minute elevation data.

b. NCEP EMC regional Eta model

The first regional model used in this study is a slightly modified version of the NCEP EMC Eta model that became operational in March 1997. For the sake of computational efficiency, the horizontal resolution was reduced from 48 km to 80 km (as used operationally until October 1995). Aside from changing the horizontal resolution, the model is almost identical to the operational version that was routinely run for 48 hours, except for procedural changes that were necessary to make longer climate integrations. The 80-km regional model integration domain used here (92x141 grid, Fig. 1a) is nearly identical to the "early" Eta 48-km domain used operationally in March 1997 (160x261 grid, not shown).

The Eta model is a state-of-the-art mesoscale weather forecast model with an accurate treatment of complex topography using the eta vertical coordinate and steplike mountains (Mesinger 1984), which eliminates errors in the pressure gradient force over steeply sloped terrain that can cause problems in sigma-coordinate models (Mesinger and Black 1992). The recent version used here follows that described by Mesinger et al. (1988), Black (1994), Rogers et al. (1995, 1996) and Mesinger (1996). The model employs a semistaggered Arakawa E-grid in which wind points are adjacent to mass points (Arakawa and Lamb 1977), configured in rotated spherical coordinates. There are 38 Eta vertical levels and the model top is at 50 hPa. Split-explicit time differencing is used with a 200-s adjustment time step.

Space differencing is done with a conserving Arakawa-type scheme (Janjic 1984). The eta steplike mountains are derived from the silhouette-mean orography of Mesinger (1995). The Eta model orography is shown in Fig. 2b.

The model physics has been described by Janjic (1990, 1994) and includes a modified Betts-Miller scheme for deep and shallow convection (Betts and Miller 1986; Janjic 1994) and predicted cloud water and ice (Zhao et al. 1997). The GFDL scheme is used for radiation (Fels and Schwarzkopf 1975; Lacis and Hansen 1974). Above the lowest model layer, free atmospheric turbulent exchange is via Mellor-Yamada (1982) level-2.5 and the surface layer similarity functions are derived from Mellor-Yamada level-2.0 (Lobocki 1993). A viscous sublayer is used over water surfaces (Janjic 1994). The land surface parameterization is a version of the Oregon State University (OSU) scheme modified by NCEP and collaborators (Chen et al. 1996, 1997), now known as the NOAH Land-Surface Model.

c. NCEP Regional Spectral Model (RSM)

The second regional model included in our intercomparison study is the NCEP Regional Spectral Model (RSM). The version of RSM used in this study is the 1997 "portable" version described by Juang et al. (1997), who summarize the changes and improvements in RSM since the original model formulation (Juang and Kanamitsu 1994). The only modifications we have made to this version are those required to perform seasonal climate integrations, namely, the periodic updating of prescribed lower boundary conditions (SST and sea ice distribution).

The RSM is a hydrostatic model that uses sigma as the vertical coordinate (a

nonhydrostatic version is also available). RSM differs from most regional models in that the variables are represented as double Fourier series over the domain of interest, while most other regional models use a grid-point representation using finite differencing to approximate spatial derivatives. Perturbation fields are computed as the difference between the RSM prognostic variables and the base fields provided by a global model or analysis. Implicit relaxation (Juang et al. 1997) is applied along the lateral boundaries to force the perturbation values to approach zero there (equivalently, the full field values approach the base field values). In operational forecast mode, a global model provides the base fields, while in our simulations, we have used NCEP/NCAR reanalysis data for the base fields.

The variables in physical space are represented on a Cartesian grid on a polar stereographic map projection. To be consistent with the other regional models, we chose the horizontal resolution to be 80 km. The domain consists of 192x107 grid points and covers a region that is similar, but not identical, to the Eta and MM5 domains (see Fig. 1). Differences in domain coverage are due to the use of different map projections and constraints on the RSM grid dimensions required for efficient fast Fourier transforms (FFTs). The vertical structure is identical to that of the NCEP/NCAR reanalysis model (28 sigma layers, with layer interfaces placed at the same values of sigma). A semi-implicit time differencing scheme is used, with a time step of 240 s.

The RSM model physics is very similar to the physics package employed in the operational NCEP global spectral model, or MRF, which is described in Hong and Pan (1996). Deep convection is parameterized using the scheme of Pan and Wu (1995), which is based on the schemes of Arakawa and Schubert (1974) and Grell (1993). Treatment of

shallow convection follows Tiedtke (1984). Grid-scale precipitation is produced by a large-scale condensation scheme. Although explicit cloud water and ice microphysics schemes are available in RSM, we decided to use the simple condensation scheme for the sake of computational efficiency. Planetary boundary layer (PBL) processes are represented using the scheme of Hong and Pan (1996) and the land surface parameterization is a modification of the Oregon State University (OSU) scheme (Mahrt and Pan 1984; Pan and Mahrt 1987; Pan 1990). For shortwave radiation, the scheme of Lacis and Hansen (1974) is used, with the Fels and Schwarzkopf (1975) scheme for longwave radiation. Cloud-radiation interaction is represented using the scheme of Slingo (1987), and gravity wave drag is parameterized following Alpert et al. (1988). The RSM orography is shown in Fig. 2c.

d. PSU/NCAR Mesoscale Model (MM5)

The third regional model we have used in this study is the Penn State/NCAR MM5. We performed seasonal integrations with two different versions of MM5, version 2-9 (released in May 1998) and version 3-2 (released in September 1999). The primary differences between the two versions will be discussed below.

The MM5 is a nonhydrostatic model that uses a modified sigma coordinate in the vertical. Rather than normalizing pressure by surface pressure, as is done with the standard σ-coordinate (Phillips 1957), the modified sigma is defined via a reference state, which is independent of time. The reference state consists of a specified vertical temperature profile and its associated hydrostatic pressure profile; once the reference state is specified, the reference surface pressure depends only on the surface topography (shown in Fig. 2d). The horizontal discretization is done on a staggered Arakawa B-grid using a Cartesian grid on a

Lambert conformal map projection. Horizontal resolution was chosen to be 80 km, consistent with the resolution of other regional models used. The domain consists of 139x105 grid points and covers a region that is similar, but not identical, to that of the Eta model (Fig. 1); differences are due to the use of different map projections. In the vertical, we chose the standard configuration using 23 layers with the model top at 50 hPa. The time discretization uses leapfrog differencing with an Asselin (1972) time filter to control the separation of solutions in time; the fundamental time step is 180 s. The semi-implicit scheme of Klemp and Wilhelmson (1978) is used to handle the terms representing fast-moving sound and gravity waves. Near the lateral boundaries, relaxation is applied to force the variables toward the specified large-scale values. For a more detailed description of the basic dynamical formulation of MM5, the reader is referred to Dudhia (1993) and Grell et al. (1994), although many physical parameterizations have been added since these works were published.

One of the notable features of MM5 is its wide selection of available physical parameterizations. In deciding which schemes to use, we generally considered two criteria: a) consistency with the other models, and b) the tradeoff between the scheme's level of sophistication and its computational efficiency. For example, in choosing a grid-scale precipitation scheme, we chose a scheme that is more sophisticated than large-scale condensation, but does not account for such phenomena as graupel and mixed-phase species (e.g., supercooled water droplets). Deep and shallow convection are parameterized using the Betts-Miller (1986) scheme, and for grid-scale precipitation the scheme of Dudhia (1989), which includes explicit cloud water and ice processes, is used. The MRF scheme (Hong and

Pan 1996) is used for PBL parameterization. The radiation parameterization of Dudhia (1989) includes a simple treatment of short- and longwave radiation and cloud-radiation interaction. There is no treatment of gravity wave drag. In Version 2, the most sophisticated land surface scheme is the force-restore slab model (Blackadar 1979; Zhang and Anthes 1982) with a 5-layer soil model (Dudhia 1996), which does not allow land surface characteristics to be modified by atmospheric and surface hydrological processes. In particular, this land surface scheme has the following serious deficiencies: a) soil moisture and albedo are fixed and depend only on the season (winter or summer) and the land use type; b) there is no representation of surface hydrology, such as runoff and snow accumulation; and c) there is no representation of sea ice. We have attempted to partially remedy the latter two shortcomings by specifying seasonally varying climatological distributions of snow cover and sea ice. Sea ice points are treated as if they were land ice, except that for sea ice the temperature at the base of the ice layer (assumed to be 47 cm thick) is constrained to be $-1.8\,^{\circ}C$, the freezing point of salt water. In Version 3, a comprehensive land surface model, the NCEP/OSU scheme of Chen et al. (1997) was added to MM5. Chen and Dudhia (2001a,b) describe the implementation of this LSM in MM5 and present some preliminary validation experiments.

e. Computational efficiency of the regional models

In this section, the computational efficiencies of the three regional models are compared. All of the Eta integrations were run on a Cray J90 at NASA/Goddard Space Flight Center, while the RSM and MM5V3 simulations were run on Cray J90s at NCAR. The MM5V2 experiments were run on a Cray C90 at NCAR. Although the models were run on

different machines using varying numbers of processors, we have attempted to give a fair comparison of their efficiency in terms of memory usage and total CPU time required per day of integration. Table 1 shows typical CPU time and memory requirements for each of the regional models, as well as the number of processors utilized and the machine type. Note that a direct comparison of the CPU time requirement for MM5V2 versus the other models is not straightforward because there is no simple proportional relationship between the execution speeds on a C90 versus a J90, although the C90 is significantly faster. We did perform test runs with RSM and MM5V2 on the same workstation, with the result that RSM required 3.5 times as much CPU time as MM5V2. However, on the workstation the RSM does not have the benefit of the Cray library fast Fourier transform (FFT) routines, which can speed up the execution of RSM by at least 33 percent, so the CPU time ratio on a Cray would likely be significantly less than 3.5.

It is apparent from Table 1 that, among the models run on the Cray J90, the Eta is the most efficient in terms of computing time. This is especially impressive in view of the fact that the Eta has more vertical levels (38) than RSM (28) and MM5 (23) and has physical parameterizations that are at least as sophisticated as the other models. For RSM, the memory requirement is large because a) the base fields must be stored over the entire integration domain, rather than along the boundaries, and b) the number of processors is a compile-time parameter that affects how arrays are dimensioned, and thus how memory is utilized. Both versions of MM5 have the lowest memory requirement, due in part to the relatively small number of vertical levels (23), although MM5V3 is relatively inefficient, using about twice as much computing time as the Eta model, though not nearly as much as

RSM.

3. Experimental design

For all of the regional model integrations, the large-scale driving fields are provided every 12 hours from NCEP/NCAR Reanalysis (Kalnay et al. 1996; Kistler et al. 2001) and linearly interpolated in time during each 12-hour interval. Although reanalysis data are available every 6 hours, we chose a 12-hour interval because data were only saved every 12 hours in our GCM integrations. The regional models are also initialized with reanalysis fields, while the COLA GCM integrations are initialized using either the NCEP reanalyses, COLA reanalyses, or operational NMC analyses (see Table 2). The reanalysis data are available in two forms: the original spectral coefficients with T62 resolution on 28 sigma levels, or evaluated on a 2.5° by 2.5° latitude-longitude grid on 17 pressure levels. For each regional model, we utilized the form of reanalysis data that is most easily handled in that particular model. All integrations for a given season begin at the same time. Aside from the time-varying lower boundary fields described below, the GCM receives no additional input after initialization, while the regional models receive only the lateral boundary fields from reanalysis.

Three summer seasons and three winter seasons were chosen for performing the experiments. The summer integrations begin in late May and extend through the end of September; the winter integrations begin in mid-December and extend through the end of March. The beginning dates and COLA GCM initialization data source for each season are given in Table 2. The winter seasons were chosen so that there would be two with

anomalous tropical Pacific SSTs (one warm and one cold) and one with near-normal tropical Pacific SSTs, while the summers were chosen so that two involved significant North American precipitation anomalies (one with drought and one with excessive precipitation) and one with near-normal precipitation over most of the region. It is important to note that in these experiments a single integration is done for each year rather than three for each year as performed by Fennessy and Shukla (2000).

Observed time-varying weekly SST (Reynolds and Smith 1994) was linearly interpolated in time (at 48-h intervals) and used in all of the integrations. The soil wetness and snow depth were predicted after initialization in the GCM, Eta, RSM and MM5V3 by their respective land surface parameterizations. Because the surface physics treatments in these models are quite different, the initializations of the snow and soil wetness are not identical, but follow the same principles. The snow cover in each model was initialized from seasonally varying climatological data. In the COLA GCM, the snow is initialized via an algorithm that derives daily snow cover and depth from the seasonal albedo data of Posey and Clapp (1954). In the Eta model, the snow is initialized via an algorithm that derives daily snow cover and depth from a 1967-1980 daily snow cover climatology calculated from the weekly NESDIS snow/ice mask. The daily distribution of sea ice in the Eta and RSM is also specified using this climatology. In RSM and MM5V3, initial snow depth is specified from the Rand monthly snow depth climatology using the month in which the initial date falls. Reanalysis snow depth has not been used due to a well-known error in its specification (snow depth for 1973 was accidentally used from 1974-1994); however, reanalysis sea ice has been used in the MM5V3 integrations. In the COLA GCM, sea ice distribution is

derived from the Reynolds and Smith (1994) SST data.

All of the integrations, except those using MM5V2, were initialized with observationally based soil wetness. The soil wetness used for initialization of the GCM integrations was derived from the operational ECMWF analysis-forecast cycle soil moisture via an algorithm described by Fennessy and Shukla (1996). The summer GCM integrations were initialized with the ECMWF derived soil wetness, while the winter GCM integrations were initialized with a 1987-1993 climatology of the ECMWF derived soil wetness. The Eta, RSM and MM5V3 integrations were all initialized with NCEP/NCAR reanalysis soil wetness.

In MM5V2, soil moisture availability is fixed in time and depends only on land use type and season (summer or winter), while snow cover (not depth) is prescribed and updated daily using the same method described above for the initial snow cover in the Eta model. Sea ice is specified daily using the same climatology used in the Eta and RSM integrations.

4. Seasonal mean climate hindcasts

To evaluate how the regional model hindcasts compare to those from the GCM, we examine seasonal mean maps for each of the models averaged over all three years for which integrations were made (Table 2). These ensembles are compared to observations averaged over the same three years. All figures show continental North America (up to 60°N) and the adjoining ocean areas, which is the main region of interest, rather than the entire domains, which are shown in Fig. 1. We also calculated mean errors and root-mean-square (RMS) errors for the ensembles and for each year over this same region, but for land points only.

In the initial stage of analysis, examination of simulated fields confirmed that the regional model simulations match the global reanalysis fields at the lateral boundaries.

a. Summer

The observed 3-year mean JJAS precipitation from a combination of station and satellite data (Xie and Arkin 1996) is shown in Fig. 3a. The corresponding ensemble mean precipitation for the GCM, Eta, RSM, MM5V3 and MM5V2 are shown in Figs. 3b-f, respectively. The model precipitation errors (with respect to the Xie-Arkin data) are shown in Fig. 4. Tables 3 and 4 show the JJAS mean errors and RMS errors of surface temperature and precipitation averaged over all the land points within the region depicted in Figs. 2 -12. To varying degrees, all of the regional models are superior to the GCM in simulating seasonal precipitation. The GCM grossly overestimates the summer precipitation over much of the continent and has ensemble mean (RMS) errors of 0.94 (1.80) mm day^{-1} (last line of Tables 3 and 4). The Eta model correctly simulates the precipitation maxima over the northwest and eastern coastal areas, as well as the overall gradient across the western Plains States and the dry conditions west of the Rocky Mountains, and has ensemble mean (RMS) errors of -0.50 (0.99) mm day^{-1}, roughly half those in the GCM. However, it fails to capture the maximum in the U.S. Midwest (which is largely due to the 1993 floods), is too wet over parts of the eastern U.S. and shows a significant dry bias over the Gulf of Mexico and over the Atlantic Ocean south of 30°N. The RSM qualitatively captures some of the observed features, but it is excessively wet over much of the region, including the eastern U.S. and most of southern Canada. It also shows a spurious maximum to the lee of the Rockies (as does the GCM and both versions of MM5) and, despite its overall moist bias, it is actually

too dry over the U.S. Midwest where a maximum was observed. The excessive wetness of the RSM is reflected in its ensemble mean (RMS) errors of 1.06 (1.71) mm day^{-1}. Both versions of MM5 have similar deficiencies, namely, excessive rainfall over the Gulf of Mexico and the Atlantic Ocean, dryness over the Deep South of the U.S., and a spurious maximum over Colorado. Both versions show a maximum over the U.S. Midwest, but its presence is probably fortuitous (see the subsequent discussion regarding the simulated circulation). Due to compensating errors over the region the MM5 ensemble mean errors are very small (-0.05 and -0.15 mm day^{-1}, respectively); the RMS errors are 1.21 and 1.16 mm day^{-1}, respectively.

The 2-meter temperature obtained from the Climate Anomaly Monitoring System (CAMS, Ropelewski et al. 1985) station data was used as the observational data set. The 3-year mean June-July-August-September (JJAS) errors for the GCM, Eta, RSM, MM5V3 and MM5V2 are shown in Figs. 5a-e, respectively. The model temperatures are adjusted using a lapse rate of 6.5°C km^{-1} for the difference between the elevation of each model grid box and the mean elevation of the stations used to form the gridded observations. It should also be noted that for both versions of MM5, the 2-meter temperature is approximated using the lowest sigma layer temperature. All of the models show significant errors of 2°C or more over portions of the continent. The most noteworthy features are the warm bias in the GCM over parts of the southwest U.S., the cold bias in the Eta and RSM over the southeast U.S., the large warm bias (exceeding 4°C in some places) in MM5V3 over most of western North America, and the significant cold bias over nearly all of North America in MM5V2. Because some of the biases compensate in the regional average, the ensemble mean errors are less

than 1 °C , with the exception of MM5V2 (Table 3). However, the ensemble RMS errors are all greater than 1 °C , though the RSM has the lowest ensemble mean and RMS errors (Table 4).

The 3-year mean JJAS 850-mb wind vectors and isotachs from NCEP/NCAR reanalysis are shown in Fig. 6a, while the simulated winds from the GCM, Eta, RSM, MM5V3 and MM5V2 are shown in Figs. 6b-f, respectively. Regions where the 850-mb surface is underground are masked out. The most prominent feature in the reanalyzed winds is the low-level jet (LLJ), which reaches the U.S. coastline as a southeasterly flow near the southern tip of Texas and curves anticyclonically through the central Great Plains, finally merging with northwesterly flow over the Great Lakes. Although a portion of the LLJ simulated by the GCM is masked out, it clearly lies to the west of its observed location. Also, the flow over the Gulf of Mexico is nearly easterly, while the observed flow is southeasterly. In the Eta model, the LLJ has the correct location and curvature but is somewhat too strong. The intensity and curvature of the LLJ in the RSM are quite realistic, but it is placed west of the observed LLJ, although not as far west as in the GCM. Both versions of MM5 give a very poor simulation of the LLJ. In MM5V2, the flow from the Gulf of Mexico has a northerly component when it reaches the Texas/Mexico coastline, and the jet is too weak and far to the west of its observed location. In MM5V3, the LLJ is also too weak, too far west and does not curve to the northeast, instead extending north and then northwest around the eastern edge of the Rockies. Finally, the westerly flow over the northeastern U.S. is well simulated by all the models except MM5; in both versions the flow is too weak.

b. Winter

The observed 3-year mean JFM Xie-Arkin precipitation is shown in Fig. 7a. The corresponding ensemble mean precipitation for the GCM, Eta, RSM, MM5V3 and MM5V2 are shown in Figs. 7b-f, respectively, and the model precipitation errors are shown in Fig. 8. Tables 5 and 6 show the JFM mean errors and RMS errors of surface temperature and precipitation averaged over all the land points within the region depicted in Figs. 2 -12. The GCM overestimates precipitation over western Texas, the northwest U.S., and especially along the coast of British Columbia. It is also too wet over portions of the Gulf of Mexico and off the Atlantic coast. The GCM shows a marked dry bias over the southeastern U.S. and has ensemble mean (RMS) errors of 0.66 (1.69) mm day^{-1} (last line of Tables 5 and 6). The Eta model correctly captures the maxima along the U.S. West Coast and over the Southeast, although the former is somewhat overestimated and the latter underestimated. As in the summer case, the Eta tends to be too dry over the Gulf of Mexico and Atlantic Ocean, but overall is very good, with ensemble mean (RMS) errors of 0.15 (0.75) mm day^{-1}. The RSM, as in summer, roughly captures the distribution of precipitation in a qualitative sense, but it produces too much precipitation over large areas of the U.S., especially in the Southern Plains and the Northwest, and has high ensemble mean (RMS) errors of 1.21 (1.53) mm day^{-1}. The two MM5 simulations are quite similar to each other; both are too wet over Texas and the southern Gulf of Mexico and too dry over the southeastern U.S. and the coast of Washington and Oregon. Their ensemble mean errors (0.42 and 0.21 mm day^{-1}) and RMS errors (1.10 and 1.11 mm day^{-1}) are between those of the GCM and the Eta.

The 3-year mean January-February-March (JFM) 2-meter temperature errors for the

GCM, Eta, RSM, MM5V3 and MM5V2 are shown in Figs. 9a-e, respectively. The model temperatures have been corrected for surface elevation differences in the manner described in section 4a. The GCM and MM5V2 show a similar error pattern, with very large warm biases (exceeding 12°C in some areas) over most of southern Canada and the U.S. Northern Plains and a cold bias of 2-4°C over much of the eastern and southern U.S. In MM5V3, the warm bias over southern Canada and parts of the northern U.S. is similar to MM5V2 and the GCM, but there is no cold bias over the eastern and southern U.S. The Eta model results show a significant cold bias (exceeding 4°C in some areas) over much of the U.S. and southern Canada, especially in the Northern Plains and the Northeast. Compared to the GCM, the Eta model shows much a much smaller warm bias over parts of western Canada. The RSM clearly has the smallest biases, with errors less than 2°C in most areas, and dramatically lower ensemble mean and RMS errors than the other models (last line of Tables 5 and 6). However, the RSM does tend to be too warm over the same areas as the GCM and both versions of MM5. We believe that the large temperature difference between the RSM and the Eta model extending from the U.S. Northern Plains to southeastern Canada, and specifically the Eta model's cold bias in this region, are due primarily to a difference in surface albedo. Examination of the mean JFM surface albedo (not shown) indicates that the Eta model's albedo exceeds that of RSM by 0.1 to 0.25 over much of the region described above. This albedo difference is in part related to the Eta model having significantly greater mean JFM snow depth than the RSM. We have found that this difference in seasonal mean snow depth is largely due to a corresponding difference in the initial snow depth, and that the algorithm in the Eta model which computes initial snow depth from initial snow cover

results in excessive snow depth over certain regions, including the one noted here. The Eta model also has a cold bias south of this region, which may be due to the advection of spuriously cold air from the area of largest cold bias.

5. Interannual variability of summer climate

In order to be useful for practical climate applications, a regional model must be able to predict features of the observed interannual variability that are due either to local boundary forcing, such as soil wetness or snow effects, or remote boundary forcing, such as SST effects that influence the regional model indirectly through the large-scale lateral boundary conditions. The interannual variability of the GCM and regional models was compared to that of the observations. In general, the regional model interannual variability is similar and perhaps somewhat improved compared to that simulated by the GCM. There is relatively more interannual variability in the precipitation scores than in the surface temperature scores, but even there, there is little correspondence between the models regarding which are the best and worst years. A case study of special interest that merits further analysis is the ability of the models to simulate the observed large differences in regional climate between the summers of 1988 and 1993.

During April, May and June of 1988, low rainfall caused a severe drought in the corn belt of the central U.S., establishing a negative soil moisture anomaly that left the region dry for the remainder of the summer. During June and July 1993, persistent heavy rainfall caused severe flooding all along the Mississippi River basin. Although each of these two unconnected events had unique characteristics and life cycles, the difference between them

is striking and presents a strong and important climatic signal that must be captured by models that are to be used for climate prediction research. A brief summary of how the GCM and regional models simulated this signal is presented here.

The 1993 versus 1988 lower boundary forcing differences for the GCM and the regional models, with the exception of MM5V2, were nearly identical. All of the models had identical SST forcing and, except for MM5V2, had similar positive 1993 minus 1988 initial soil wetness differences in the corn belt of the U.S. (not shown). (Recall that soil moisture depends only on season and land use category in MM5V2.)

The observed June-July mean 1993 minus 1988 precipitation difference is shown in Fig. 10a. The corresponding precipitation differences for the GCM, Eta, RSM, MM5V3 and MM5V2 are shown in Figs. 10b-f, respectively. Prominent in the observations is a broad 1 mm d^{-1} positive precipitation difference that spans much of the central U.S. and reaches over 4 mm d^{-1} over the upper Mississippi basin. The GCM does not capture this signal at all, but rather has weaker positive differences both eastward and southward of the observed positive difference. The Eta model does a better job of placing the positive difference in approximately its observed location and captures its extension to the northwest into southwestern Canada, but the signal is weaker than observed nearly everywhere, and the area covered by the positive differences is also smaller than observed. The RSM shows a positive difference over parts of the central Midwest and Northern Plains, but the signal is too weak over the central Midwest and does not cover parts of the observed area of positive differences. In addition, the RSM has erroneous negative differences over most of the central and southern Plains and large spurious positive differences over much of eastern

Canada. Neither version of MM5 gives a good simulation of this signal. In both versions, the precipitation difference pattern is noisy and incoherent. In MM5V2, parts of the central Plains and southern Mississippi Valley have positive differences, but there is a very large negative difference over the northern Mississippi Valley where flooding occurred. MM5V3 shows an even less coherent pattern in the central U.S. as well as spurious negative differences over the mid-Atlantic region. We believe that these poor simulations of the precipitation difference signal are linked to the complete failure of both versions of MM5 to capture the difference in low-level winds (see the discussion below). Finally, both versions of MM5 show large positive differences along and offshore from the Gulf and Atlantic coasts, contrary to observations.

The observed June-July mean 2-meter temperature difference for 1993 minus 1988 is shown in Fig. 11a. The corresponding temperature differences for the GCM, Eta, RSM, MM5V3 and MM5V2 are shown in Figs. 11b-f, respectively. The prominent feature in the observations is the large area of relatively colder temperatures for 1993 extending from the Great Lakes to the Pacific coast north of 40°N. All of the models capture this signal to varying degrees, but with an incorrect magnitude, location, or both. In the GCM, the region of negative differences extends well to the south of the observed region and the signal is too weak over the northern Plains and Rockies. The Eta model produces a stronger signal, but places it too far west and extends it too far east (across the Great Lakes and into the Northeast). The Eta also fails to produce negative differences over the western Plains. The RSM shows an even stronger signal than the Eta, but centers it somewhat north of its observed location, and there is a large region of spurious positive differences over the

southern and western Plains, the same region where the RSM showed an incorrect negative precipitation difference. In MM5V2, the temperature difference signal has the correct magnitude but is centered over the Great Lakes, far to the east of the observed pattern. The MM5V3 signal is centered well to the southeast of observed, is too weak, and extends too far to the east, into southeastern Canada.

The June-July mean 1993 minus 1988 850-mb wind vectors and isotachs from the NCEP/NCAR reanalysis are shown in Fig. 12a. The corresponding model winds for the GCM, Eta, RSM, MM5V3 and MM5V2 are shown in Figs. 12b-f, respectively. Two notable features are apparent in the observations. The wind difference signal over the south-central U.S. indicates that the low-level jet (LLJ) was much stronger in 1993 than in 1988; it is obvious that the moisture transport from this enhanced LLJ was a major factor in the 1993 floods. Another feature worth noting is the relative strength of the Pacific high in 1993 relative to 1988; this is evidenced by the relative northerly, anticyclonically curving winds off the Pacific coast. The GCM completely failed to capture either of these features. In the Eta model, the LLJ signal is weakly captured over Texas, but the feature does not extend to the northeast as observed. The circulation difference for the Pacific high also has the wrong sense. The RSM produces a fairly good simulation of the LLJ signal, although it is slightly weaker and placed somewhat to the northwest of the observed pattern. The RSM Pacific high signal is very weak but has the correct orientation. In both versions of MM5, the simulation of these two features bears no resemblance to the observations. In MM5V2, the flow difference over the Mississippi Valley is nearly opposite to that observed, the Pacific high circulation difference is nearly as strong as observed but in the opposite direction, and

there is a jetlike feature off the Southeast coast which is completely erroneous. In MM5V3, there is a very weak difference signal over the Southern Plains that is in the wrong direction, the Pacific high circulation difference is in the wrong sense, and as in MM5V2, there is a spurious jet feature off the South Atlantic coast. It is clear that both versions of MM5 have completely failed to capture the low-level wind differences between 1988 and 1993, just as they failed to give a good simulation of the precipitation difference signal.

6. Summary and conclusions

In this study, we have compared the abilities of three regional models (NCEP Eta, NCEP RSM, and two versions of the PSU/NCAR MM5), as well as the COLA GCM, to simulate seasonal mean climate over North America for both summer and winter. In addition, in order to assess the models' ability to simulate interannual variability in summer, we have examined the differences in simulated climate between the anomalous 1988 and 1993 summer seasons.

Based on the mean and RMS error scores presented in Tables 3-6, it can be concluded that all of the regional models, with the exception of RSM, show greater skill in simulating seasonal mean precipitation than the GCM in both summer and winter. Overall, the Eta model yields the best results for precipitation. Because the RSM was able to capture the qualitative distribution of precipitation reasonably well, it is clear that it would give much better precipitation scores were its substantial moist bias reduced.

The RSM clearly shows the greatest skill in simulating seasonal mean surface temperature in summer and winter, especially the latter. Of the models presented here, it

alone is free of major warm or cold biases over most of the domain in winter. The comparison between the temperature results of the other models is less clear-cut; all exhibit marked biases over much of the region in both seasons. Two other results are worth stating here: a) the degradation of the Eta model's performance is largely due to a systematic cold bias in both seasons; its reduction could make the Eta more competitive with RSM, and b) both versions of MM5 are somewhat better than the GCM and Eta in winter, but are significantly worse in summer.

To evaluate the models' ability to simulate lower tropospheric circulation in summer, we compared their simulated 850-mb wind fields, particularly the low-level jet (LLJ) which is an important feature of the summer circulation. The Eta and RSM both capture the LLJ more skillfully than the other models, although both have deficiencies. The GCM gives a less satisfactory simulation of the LLJ, and it is very poorly simulated in both versions of MM5.

To evaluate the models' ability to capture interannual variability in the summer season, we compared the simulated June-July 1993 minus 1988 precipitation, surface temperature and 850-mb circulation. In general, none of the models display marked skill in capturing this important climatic signal. For precipitation, only the Eta and RSM show a pattern that bears any resemblance to the observations, although both have serious deficiencies, especially the RSM. Neither the GCM nor either version of MM5 reproduce the observed precipitation signal in any way. The surface temperature signal is better simulated than the precipitation signal; all of the models were able to reproduce the temperature difference with the correct sign, although the magnitude and/or location of the

pattern are erroneous in each case. It is not clear which of the models is best at capturing the temperature signal. Finally, in simulating the difference in 850-mb circulation, the RSM clearly produces the best result, capturing the enhanced LLJ in 1993 versus 1988. Of the remaining models, only the Eta weakly captures the observed difference in the LLJ. It is apparent that the MM5's failure to simulate the observed precipitation difference is linked to its inability to capture the difference in lower tropospheric circulation.

Taking into account the models' individual performance as well as their computational efficiency (Sec. 2e), it is apparent that the Eta model provides the most favorable combination of performance and efficiency. Although the RSM performs very well in some respects, it is more than twice as expensive as the Eta, and its moist bias is a significant drawback. Given their performance, neither version of MM5 would appear to be competitive with the Eta and RSM for climate simulations even if they were computationally efficient, which they are not, at least when compared to the Eta model.

Although this study has shed light on some important modeling questions, it raises several others. In particular, why are the MM5 simulations so poor? Despite the coupling of the OSU LSM to MM5V3, this version's performance is not markedly superior to that of MM5V2. We offer two possible explanations. First, MM5 does not include any parameterization of gravity wave drag. Although it may be relatively unimportant in short-term weather phenomena, which MM5 has traditionally been used to study, gravity wave drag can be an important contributor to the momentum balance in longer-term simulations. Secondly, the radiation parameterization used in both versions of MM5 is relatively simple and designed for computational efficiency, and perhaps is not well suited to climate

simulations. It is also possible that other features of MM5 are better suited to simulations of phenomena on different time and spatial scales than studied here.

An even more important question concerns the fact that the Eta model, nested in the COLA GCM (Fennessy and Shukla 2000), gives a markedly better simulation of the summer 1988 versus 1993 climate signal than the same model forced by reanalysis data in the present study. Recently, we have performed a new set of integrations with a more recent version of the Eta model, using lateral boundary conditions from reanalysis and also from a revised version of the COLA GCM, for the same three summer and three winter seasons studied in this paper. The GCM-forced integrations are five-member ensembles. Comparison of GCM- and reanalysis-forced results has also shown that the GCM-forced Eta model captures the 1993 minus 1988 signal better than the reanalysis-forced model. This topic will be addressed in a forthcoming paper.

Acknowledgments. We are thankful for useful discussions with Prof. F. Mesinger on aspects of the Eta model. We also thank W. Wang and K. Manning of NCAR/MMM for their assistance with MM5. The model integrations discussed here were done on computers at the NASA Center for Computational Sciences at Goddard Space Flight Center and at NCAR. This research was supported by NSF Grant ATM-9814295, NOAA Grant NA-96GP0056 and NASA Grant NAG5-8202.

References

Alpert, J. C., M. Kanamitsu, P. M. Caplan, J. G. Sela, G. H. White and E. Kalnay, 1988: Mountain induced gravity wave drag parameterization in the NMC medium-range forecast model. Proceedings of the Eighth AMS Conference on Numerical Weather Prediction, 22-26 February 1988, AMS, Boston, MA, 726-733.

Arakawa, A., and V. R. Lamb, 1977: Computational design of the basic dynamical processes of the UCLA general circulation model. *Methods Comput. Phys.*, **17**, 173-265.

Arakawa, A., and W. H. Schubert, 1974: Interaction of cumulus cloud ensemble with the large-scale environment. *J. Atmos. Sci.*, **31**, 671-701.

Asselin, R., 1972: Frequency filter for time-integrations. *Mon. Wea. Rev.*, **100**, 487-490.

Betts, A. K., and M. T. Miller, 1986: A new convective adjustment scheme. Part II: Single column tests using GATE wave, BOMEX, and Arctic air-mass data. *Q. J. Roy. Meteor. Soc.*, **112**, 693-703.

Black, T., 1994: The new NMC mesoscale Eta model: Description and forecast examples. *Wea. Forecasting*, **9**, 265-278.

Blackadar, A. K., 1979: High resolution models of the planetary boundary layer. *Advances in Environmental Science and Engineering*, 1, No. 1. Pfafflin and Ziegler, Eds., Gordon and Briech Sci. Publ., New York, 50-85.

Chen, F., and J. Dudhia, 2001a: Coupling an advanced land surface-hydrology model with the Penn State-NCAR MM5 modeling system. Part I: Model implementation and sensitivity. *Mon. Wea. Rev.*, **129**, 569-585.

Chen, F., and J. Dudhia, 2001b: Coupling an advanced land surface-hydrology model with the Penn State-NCAR MM5 modeling system. Part II: Preliminary model validation. *Mon. Wea. Rev.*, **129**, 587-604.

Chen, F., K. Mitchell, J. Schaake, Y. Xue, H.-L. Pan, V. Koren, Q. Y. Duan, K. Ek, and A. Betts, 1996: Modeling of land-surface evaporation by four schemes and comparison with FIFE ovservations. *J. Geophys. Res.*, **101**, 7251-7268.

Chen, F., Z. Janjic and K. Mitchell, 1997: Impact of atmospheric surface layer parameterization in the new land-surface scheme of the NCEP mesoscale Eta numerical model. *Bound.-Layer Meteor.*, **85**, 391-421.

DeWitt, D. G., 1996: The effect of cumulus convection on the climate of COLA general

circulation model. *COLA Technical Report #27*. Available from Center for Ocean-Land-Atmosphere Studies, 4041 Powder Mill Road, Suite 302, Calverton, MD 20705.

Dorman, J. L., and P. Sellers, 1989: A global climatology of albedo, roughness length and stomatal resistance for atmospheric general circulation models as represented by the Simple Biosphere Model (SiB). *J. Appl. Meteor.*, **28**, 833-855.

Dudhia, J., 1989: Numerical study of convection observed during the winter monsoon experiment using a mesoscale two-dimensional model. *J. Atmos. Sci.*, **46**, 3077-3107.

Dudhia, J., 1993: A nonhydrostatic version of the Penn State/NCAR mesoscale model: Validation tests and simulation of an Atlantic cyclone and cold front. *Mon. Wea. Rev.*, **121**, 1493-1513.

Dudhia, J., 1996: A multi-layer soil temperature model for MM5. *Preprints, The Sixth PSU/NCAR Mesoscale Model Users Workshop*, 22-24 July 1996, Boulder, CO, 49-50.

Fels, S. B., and M. D. Schwarzkopf, 1975: The simplified exchange approximation: A new method for radiative transfer calculations. *J. Atmos. Sci.*, **32**, 1475-1488.

Fennessy, M. J., and J. Shukla, 1996: Impact of initial soil wetness on seasonal atmospheric prediction. *COLA Technical Report #34*. Available from Center for Ocean-Land-Atmosphere Studies, 4041 Powder Mill Road, Suite 302, Calverton, MD 20705.

Fennessy, M. J., and J. Shukla, 2000: Seasonal prediction over North America with a regional model nested in a global model. *J. Climate*, **13**, 2605-2627.

Fennessy, M. J., and Y. Xue, 1997: Impact of USGS vegetation map on GCM simulations over the United States. *Ecological Applications*, **7**, 22-23.

Giorgi, F., 1990: Simulation of regional climate using a limited area model nested in a general circulation model. *J. Climate*, **3**, 941-963.

Giorgi, F., and G. T. Bates, 1989: The climatological skill of a regional model over complex terrain. *Mon. Wea. Rev.*, **117**, 2325-2347.

Grell, G. A., 1993: Prognostic evaluation of assumptions used by cumulus parameterization. *Mon. Wea. Rev.*, **121**, 764-787.

Grell, G. A., J. Dudhia, and D. R. Stauffer, 1994: A description of the fifth-generation Penn State/NCAR mesoscale model (MM5). *NCAR Technical Note*, NCAR/TN-398+STR,

117 pp.

Harshvardhan, R. Davies, D. A. Randall and T. G. Corsetti, 1987: A fast radiation parameterization for general circulation models. *J. Geophys. Res.*, **92**, 1009-1016.

Hogan, T. F., and T. E. Rosmond, 1991: The description of the Navy operational global atmospheric prediction system's spectral forecast model. *Mon. Wea. Rev.*, **119**, 1786-1815.

Hong, S.-Y., H.-M. H. Juang, and D.-K. Lee, 1999: Evaluation of a regional spectral model for the East Asian monsoon case studies for July 1987 and 1988. *J. Meteor. Soc. Japan*, **77**, 553-572.

Hong, S.-Y., and A. Leetmaa, 1999: An evaluation of the NCEP RSM for regional climate modeling. *J. Climate*, **12**, 592-609.

Hong, S.-Y., and H.-L. Pan, 1996: Nonlocal boundary layer vertical diffusion in a medium-range forecast model. *Mon. Wea. Rev.*, **124**, 2322-2339.

Hou, Y.-T., 1990: Cloud-Radiation-Dynamics Interaction. Ph.D. Thesis, Dept. of Meteorology, University of Maryland, College Park, MD 20742.

Janjic, Z. I., 1984: Nonlinear advection schemes and energy cascade on semi-staggered grids. *Mon. Wea. Rev.*, **112**, 1234-1245.

Janjic, Z. I., 1990: The step-mountain coordinate: physical package. *Mon. Wea. Rev.*, **118**, 1429-1443.

Janjic, Z. I., 1994: The step-mountain Eta coordinate model: further developments of convection, viscous sublayer, and turbulence closure schemes. *Mon. Wea. Rev.*, **122**, 927-945.

Ji, Y., 1996: Modeling the Asian summer monsoon with high resolution regional Eta model: The impact of sea surface temperature anomaly associated with ENSO cycle. Ph.D. dissertation, University of Maryland at College Park, 139 pp. [Available from University Microfilm, The University of Maryland at College Park, College Park, MD 20742.]

Ji, Y., and A. D. Vernekar, 1997: Simulation of the Asian summer monsoons of 1987 and 1988 with a regional model nested in a global GCM. *J. Climate*, **10**, 1965-1979.

Juang, H.-M. H., S.-Y. Hong, and M. Kanamitsu, 1997: The NCEP regional spectral model: An update. *Bull. Amer. Meteor. Soc.*, **78**, 2125-2143.

Juang, H.-M. H., and M. Kanamitsu, 1994: The NMC regional spectral model. *Mon. Wea. Rev.*, **122**, 3-26.

Kalnay, E., and Co-authors, 1996: The NCEP/NCAR 40-year reanalysis project. *Bull. Amer. Meteor. Soc.*, **77**, 437-471.

Kinter, J. L. III, J. Shukla, L. Marx and E. K. Schneider, 1988: A simulation of the winter and summer circulations with the NMC global spectral model. *J. Atmos. Sci.*, **45**, 2486-2522.

Kinter, J. L. III, D. DeWitt, P. A. Dirmeyer, M. J. Fennessy, B. P. Kirtman, L. Marx, E. K. Schneider, J. Shukla and D. M. Straus, 1997: The COLA atmosphere-biosphere general circulation model. Volume I: Formulation. *COLA Technical Report #51.* Available from Center for Ocean-Land-Atmosphere Studies, 4041 Powder Mill Road, Suite 302, Calverton, MD 20705.

Kistler, R., and Co-authors, 2001: The NCEP-NCAR 50-year reanalysis: Monthly means CD-ROM and documentation. *Bull. Amer. Meteor. Soc.*, **82**, 247-267.

Klemp, J. B., and R. B. Wilhelmson, 1978: Simulations of three-dimensional convective storm dynamics. *J. Atmos. Sci.*, **35**, 1070-1096.

Lacis, A. A., and J. E. Hansen, 1974: A parameterization for the absorption of solar radiation in the earth's atmosphere. *J. Atmos. Sci.*, **31**, 118-133.

Lobocki, L., 1993: A procedure for the derivation of surface-layer bulk relationships from simplified second-order closure models. *J. Appl. Meteor.*, **32**, 126-138.

Mahrt, L., and H.-L. Pan, 1984: A two layer model of soil hydrology. *Bound.-Layer Meteor.*, **29**, 1-20.

Mellor, G. L., and T. Yamada, 1982: Development of a turbulence closure model for geophysical fluid problems. *Rev. Geophys. Space Phys.*, **20**, 851-875.

Mesinger, F., 1984: A blocking technique for representation of mountains in atmospheric models. *Riv. Meteor. Aeronaut.*, **44**, 195-202.

Mesinger, F., 1995: The eta regional model and its performance at the U.S. National Centers for Environmental Prediction. *Int. Workshop on Limited-Area and Variable Resolution Models*, Beijing, China, World Meteorological Organization, 19-28.

Mesinger, F., 1996: Improvements in quantitative precipitation forecasts with the Eta

regional model at the National Centers for Environmental Prediction: The 48-km upgrade. *Bull. Amer. Meteor. Soc.*, **77**, 2637-2649.

Mesinger, F., and T. L. Black, 1992: On the impact of forecast accuracy of the step-mountain (eta) vs. sigma coordinate. *Meteor. Atmos. Phys.*, **50**, 47-60.

Mesinger, F., Z. I. Janjic, S. Nickovic, D. Gavrilov and D. G. Deaven, 1988: The step-mountain coordinate: Model description and performance for cases of Alpine lee cyclogenesis and for a case of an Appalachian redevelopment. *Mon. Wea. Rev.*, **116**, 1493-1518.

Miyakoda, K., and J. Sirutis, 1977: Comparative integrations of global spectral models with various parameterized processes of subgrid scale vertical transports. *Beitr. Phys. Atmos.*, **50**, 445-447.

Moorthi, S., and M. J. Suarez, 1992: Relaxed Arakawa-Schubert: A parameterization of moist convection for general circulation models. *Mon. Wea. Rev.*, **120**, 978-1002.

Pan, H.-L., 1990: A simple parameterization scheme of evapotranspiration over land for the NMC medium-range forecast model. *Mon. Wea. Rev.*, **118**, 2500-2512.

Pan, H.-L., and L. Mahrt, 1987: Interaction between soil hydrology and boundary layer developments. *Bound-Layer Meteor.*, **38**, 185-202.

Pan, H.-L., and W.-S. Wu, 1995: Implementing a mass flux convective parameterization package for the NMC medium-range forecast model. NMC Office Note 409, 40 pp. [Available from NCEP/EMC, 5200 Auth Road, Camp Springs, MD 20746.]

Phillips, N. A., 1957: A coordinate system having some special advantages for numerical forecasting. *J. Meteor.*, **14**, 184-185.

Posey, J. W., and P. F. Clapp, 1954: Global distribution of normal surface albedo. *Geofisica Int.*, **4**, 33-48.

Reynolds, R. W., and T. M. Smith, 1994: Improved global sea surface temperature analyses using optimum interpolation. *J. Climate*, **7**, 929-948.

Rogers, E., T. L. Black, D. G. Deaven, G. J. DiMego, Q. Zhao, M. Baldwin, N. W. Junker and Y. Lin, 1996: Changes to the operational "early" Eta analysis/forecast system at the National Centers for Environmental Prediction. *Wea. Forecasting*, **11**, 391-413.

Rogers, E., D. G. Deaven, and G. J. DiMego, 1995: The regional analysis system for the operational "early" Eta model: Original 80-km configuration and recent changes.

Wea. Forecasting, **10**, 810-825.

Ropelewski, C. F., J. E. Janowiak, and M. F. Halpert, 1985: The analysis and display of real time surface climate data. *Mon. Wea. Rev.*, **113**, 1101-1107.

Sato, N., P. J. Sellers, D. A. Randall, E. K. Schneider, J. Shukla, J. L. Kinter III, Y.-T. Hou, and E. Albertazzi, 1989: Effects of implementing the Simple Biosphere Model in a general circulation model. *J. Atmos. Sci.*, **46**, 2757-2782.

Sela, J. G., 1980: Spectral modeling at the National Meteorological Center. *Mon. Wea. Rev.*, **108**, 1279-1292.

Sellers, P. J., Y. Mintz, Y. C. Sud, and A. Dalcher, 1986: A simple biosphere model (SiB) for use within general circulation models. *J. Atmos. Sci.*, **43**, 505-531.

Shukla, J., 1998: Predictability in the midst of chaos: A scientific basis for climate forecasting. *Science*, **282**, 728-731.

Slingo, J., 1987: The development and verification of a cloud prediction scheme for the ECMWF model. *Q. J. Roy. Meteor. Soc.*, **103**, 29-43.

Tanajura, C., 1996: Modeling and analysis of the South American summer climate. Ph.D. dissertation, University of Maryland.

Tiedtke, M., 1984: The effect of penetrative cumulus convection on the large-scale flow in a general circulation model. *Beitr. Phys. Atmos.*, **57**, 216-239.

Vernekar, A., B. Kirtman, J. Zhou, and D. DeWitt, 1992: Orographic gravity-wave drag effects on medium-range forecasts with a general circulation model. **Physical Processes in Atmospheric Models**, Editors: D. R. Sikka and S. S. Singh, Wiley Eastern Limited, New Delhi, 295-307.

Xie, P., and P. Arkin, 1996: Analysis of global monthly precipitation using gauge observations, satellite estimates, and numerical model predictions. *J. Climate*, **9**, 840-858.

Xue, Y., P. J. Sellers, J. L. Kinter, and J. Shukla, 1991: A simplified biosphere model for global climate studies. *J. Climate*, **4**, 345-364.

Zhang, D.-L., and R. A. Anthes, 1982: A high-resolution model of the planetary boundary layer—sensitivity tests and comparisons with SESAME-79 data. *J. Appl. Meteor.*, **21**, 1594-1609.

Zhao, Q., T. L. Black, and M. E. Baldwin, 1997: Implementation of the cloud prediction scheme in the Eta model at NCEP. *Wea. Forecasting*, **12**, 697-711.

TABLE 1. Total CPU time required in minutes per day of integration, maximum memory usage in megawords (Mw), number of processors utilized, and type of machine used.

Model	Eta	RSM	MM5V3	MM5V2
CPU (min/d)	99	230	200	50†
Memory (Mw)	42	67	26	25
Processors	12	9	16	8
Machine Type	Cray J90	Cray J90	Cray J90	Cray C90

†The CPU time required on a Cray C90 is not directly comparable to that on a J90

TABLE 2. Integration initial dates and GCM initialization data sources.

Summer Integrations		**Winter Integrations**	
00UTC 28 May 1987	NMC Analysis	00UTC 13 Dec 1982	COLA Reanalysis
00UTC 28 May 1988	NMC Analysis	00UTC 13 Dec 1988	NCEP Reanalysis
00UTC 28 May 1993	NMC Analysis	00UTC 13 Dec 1990	NCEP Reanalysis

TABLE 3. JJAS mean error averaged over 142°W-60°W, 20°N-60°N, land only, for each year and the 3-year ensemble (E).

Yr	Surface Temperature (°C)					Precipitation (mm day^{-1})				
	GCM	Eta	RSM	MM5 V3	MM5 V2	GCM	Eta	RSM	MM5 V3	MM5 V2
87	0.21	-0.98	0.39	0.35	-2.57	0.99	-0.29	1.04	0.04	-0.07
88	0.59	-0.68	0.10	1.43	-1.99	0.98	-0.56	1.05	0.14	0.02
93	0.41	-0.63	0.27	1.04	-2.18	0.86	-0.65	1.08	-0.33	-0.37
E	0.40	-0.76	0.25	0.94	-2.25	0.94	-0.50	1.06	-0.05	-0.14

TABLE 4. JJAS root mean square (RMS) error averaged over 142°W-60°W, 20°N-60°N, land only, for each year and the 3-year ensemble (E).

Yr	Surface Temperature (°C)					Precipitation (mm day^{-1})				
	GCM	Eta	RSM	MM5 V3	MM5 V2	GCM	Eta	RSM	MM5 V3	MM5 V2
87	1.67	1.95	1.45	1.87	2.92	1.89	0.93	1.79	1.35	1.11
88	1.78	1.66	1.65	2.30	2.35	1.97	1.23	1.68	1.60	1.57
93	1.59	1.79	1.76	2.53	2.80	1.96	1.29	2.13	1.72	1.40
E	1.47	1.59	1.41	2.00	2.58	1.80	0.99	1.71	1.21	1.16

TABLE 5. JFM mean error averaged over 142°W-60°W, 20°N-60°N, land only, for each year and the 3-year ensemble (E).

Yr	Surface Temperature (°C)					Precipitation (mm day^{-1})				
	GCM	Eta	RSM	MM5 V3	MM5 V2	GCM	Eta	RSM	MM5 V3	MM5 V2
83	2.55	-2.03	1.06	1.27	0.70	0.45	0.35	1.42	0.50	0.10
89	1.76	-2.35	0.13	2.21	1.69	0.74	0.02	1.14	0.37	0.40
91	0.71	-2.68	-0.01	1.36	-0.25	0.77	0.08	1.08	0.40	0.12
E	1.67	-2.35	0.39	1.61	0.71	0.66	0.15	1.21	0.42	0.21

TABLE 6. JFM root mean square (RMS) error averaged over 142°W-60°W, 20°N-60°N, land only, for each year and the 3-year ensemble (E).

Yr	Surface Temperature (°C)					Precipitation (mm day^{-1})				
	GCM	Eta	RSM	MM5 V3	MM5 V2	GCM	Eta	RSM	MM5 V3	MM5 V2
83	5.32	3.15	2.42	3.76	4.00	2.29	1.38	1.98	1.87	1.55
89	3.96	3.60	1.88	4.13	3.99	1.47	0.81	1.70	1.04	1.30
91	3.83	3.50	1.83	2.54	2.38	1.76	1.01	1.42	1.16	1.11
E	4.14	3.20	1.57	3.27	3.23	1.69	0.75	1.53	1.10	1.11

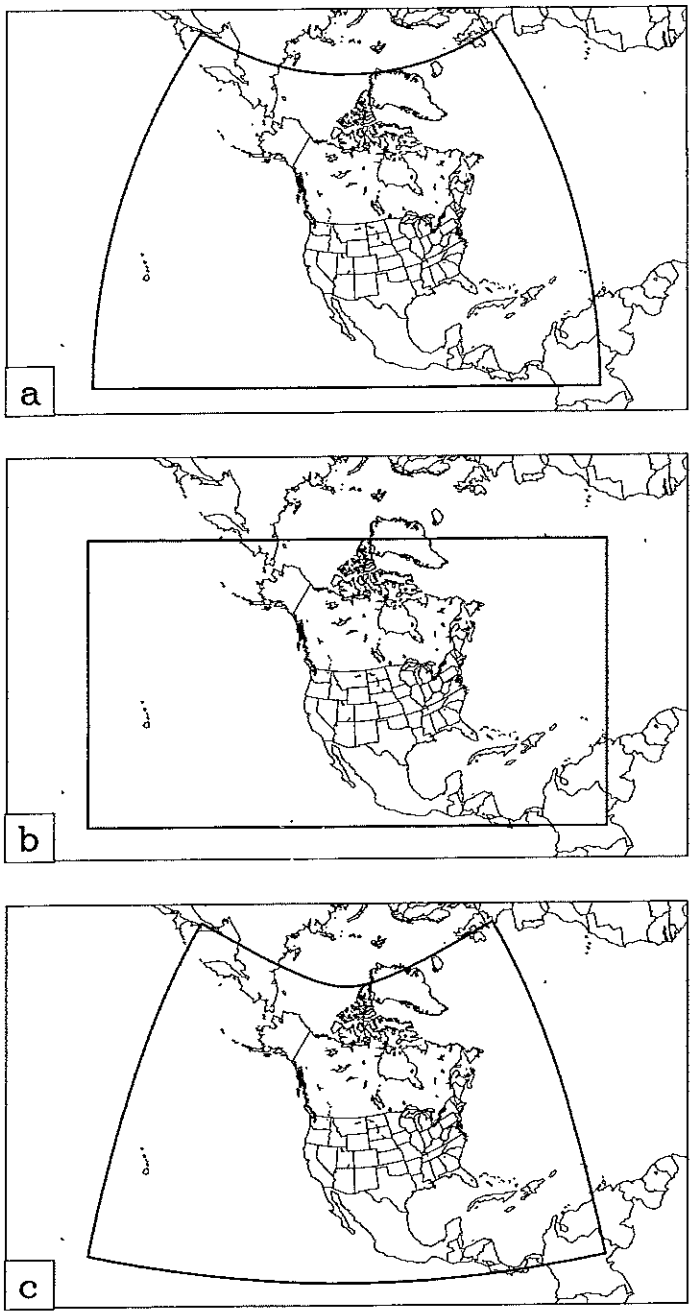

Fig. 1. Integration domain of a) Eta, b) RSM and c) MM5V3. Each model has 80-km horizontal resolution.

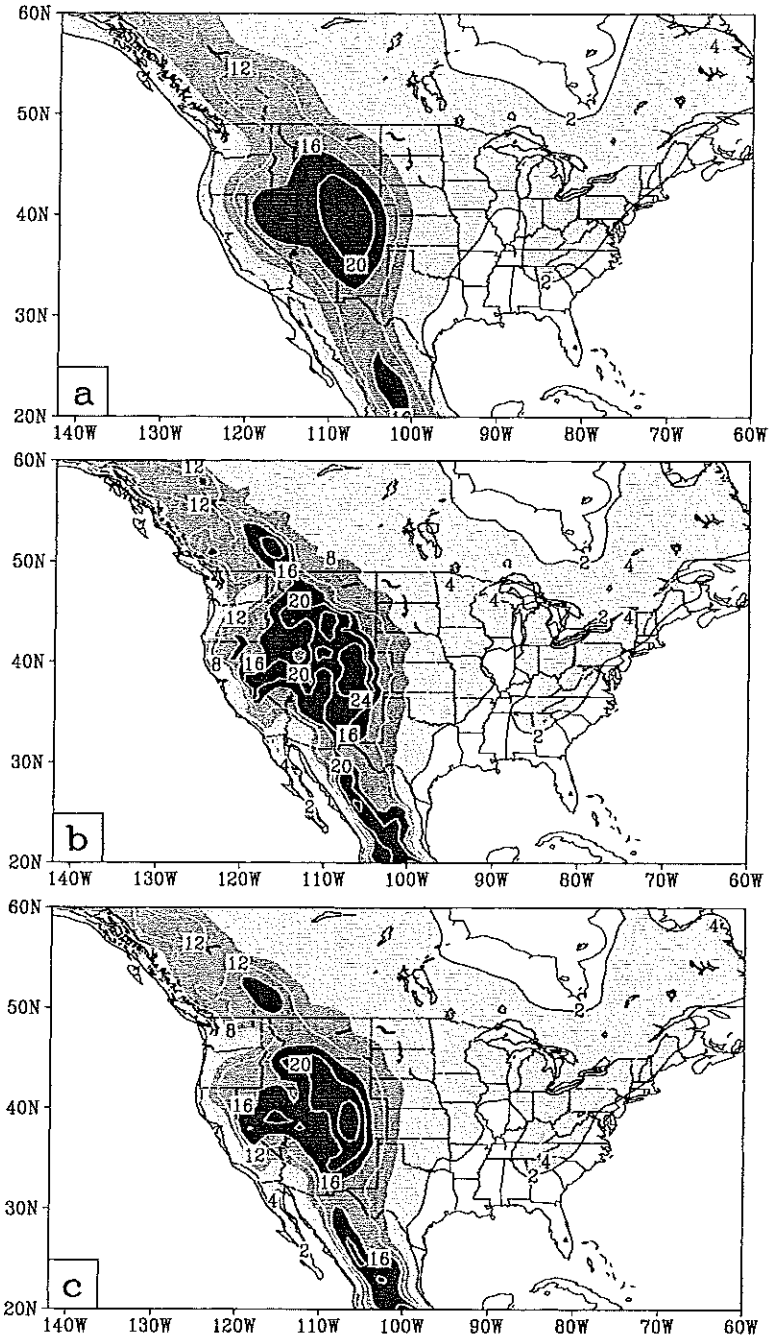

Fig. 2. Orography used in a) COLA GCM, b) Eta, c) RSM and d) MM5V3. Units are in hundreds of meters and contours are 2, 4, 8, 12, 16, 20, 24.

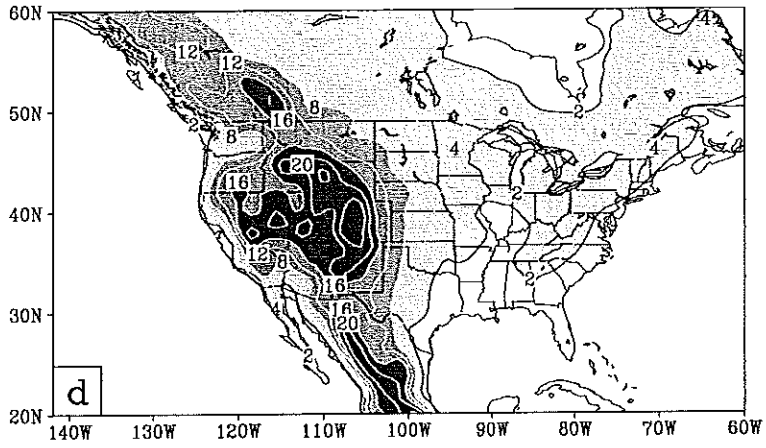

Fig. 2 (continued)

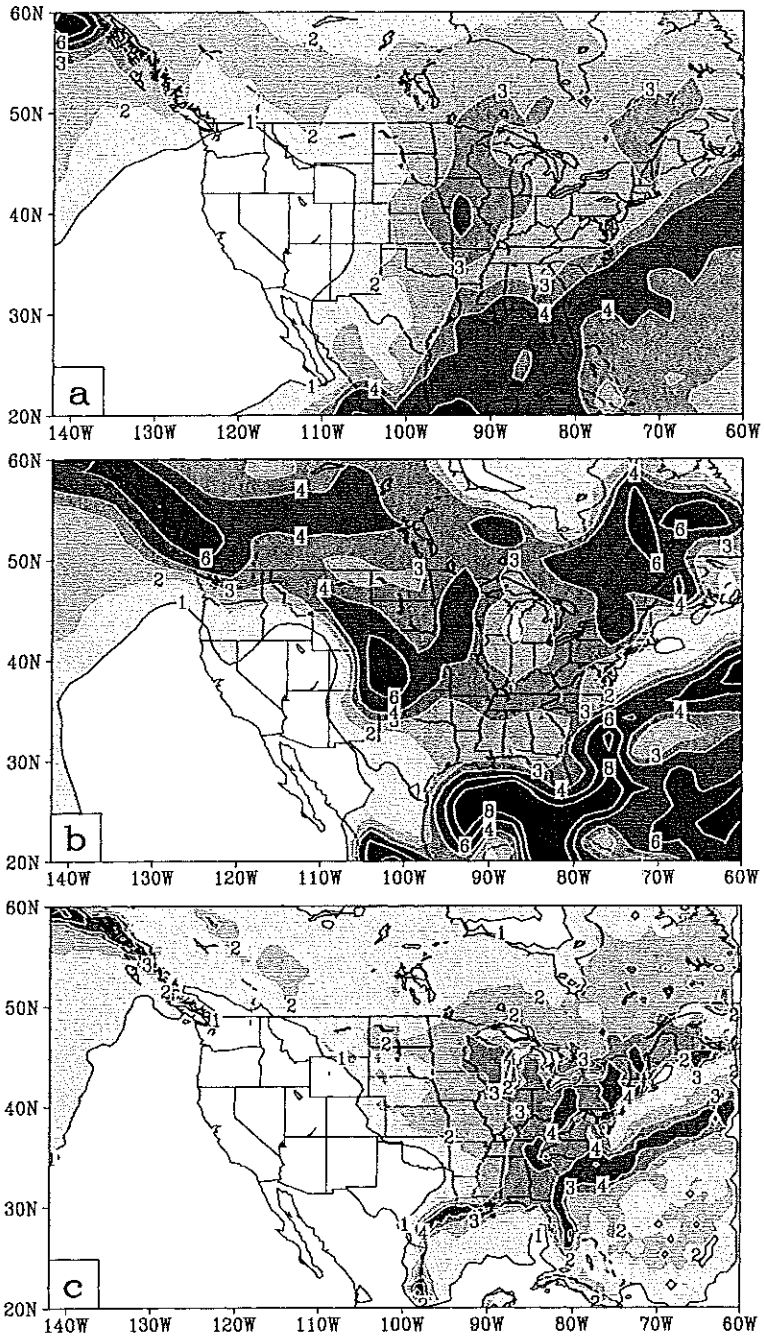

Fig. 3. JJAS 3-year mean precipitation for a) Xie-Arkin observations, b) COLA GCM, c) Eta, d) RSM, e) MM5V3 and f) MM5V2. Contours are 1, 2, 3, 4, 6, 8 mm d^{-1}.

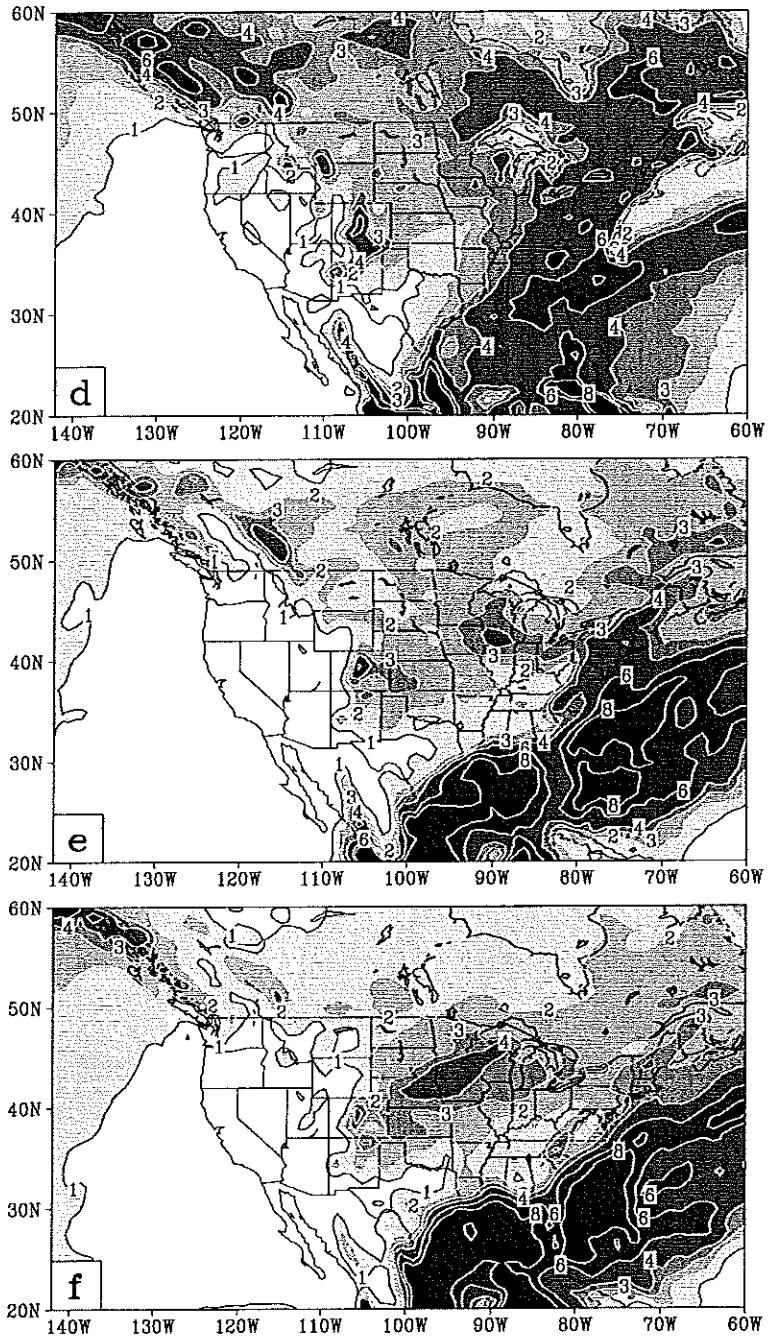

Fig. 3 (continued)

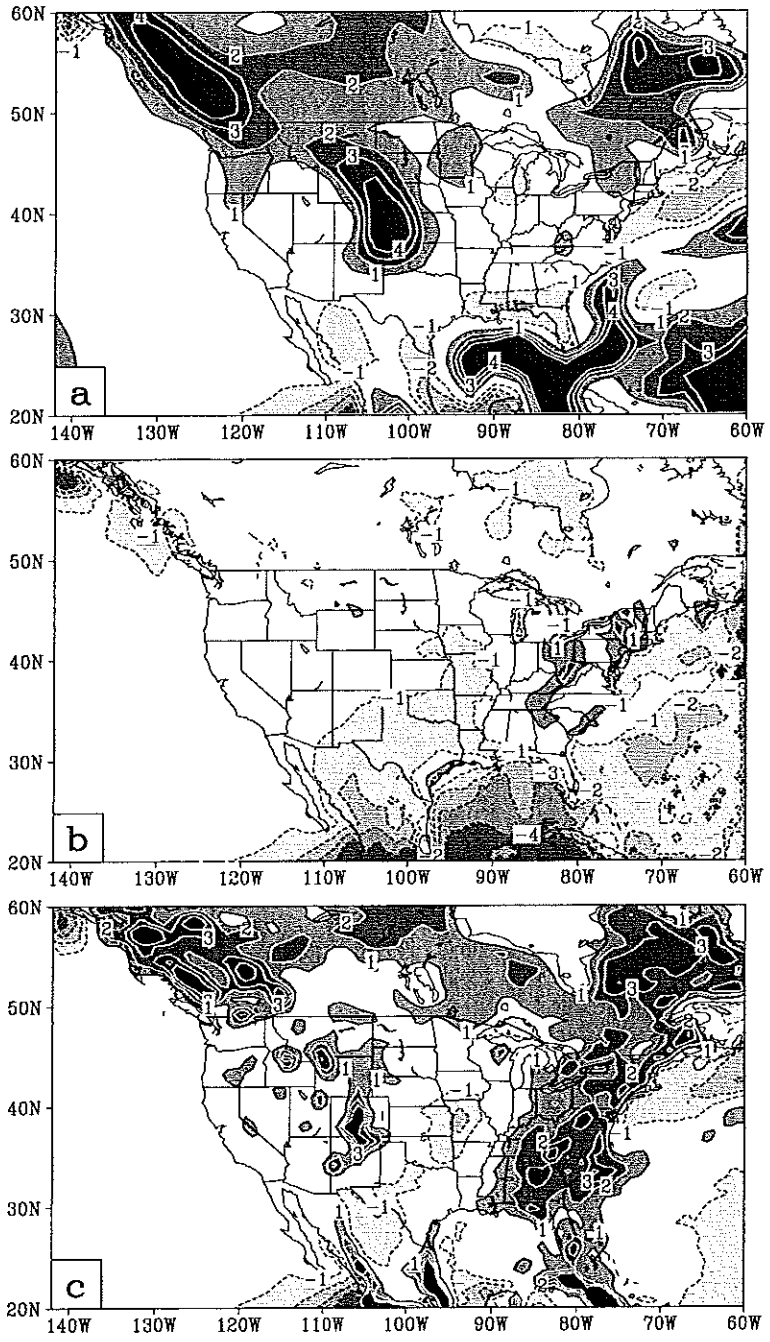

Fig. 4. JJAS 3-year mean precipitation error for a) COLA GCM, b) Eta, c) RSM, d) MM5V3 and e) MM5V2. Contours are ±1, 2, 3, 4 mm d^{-1}.

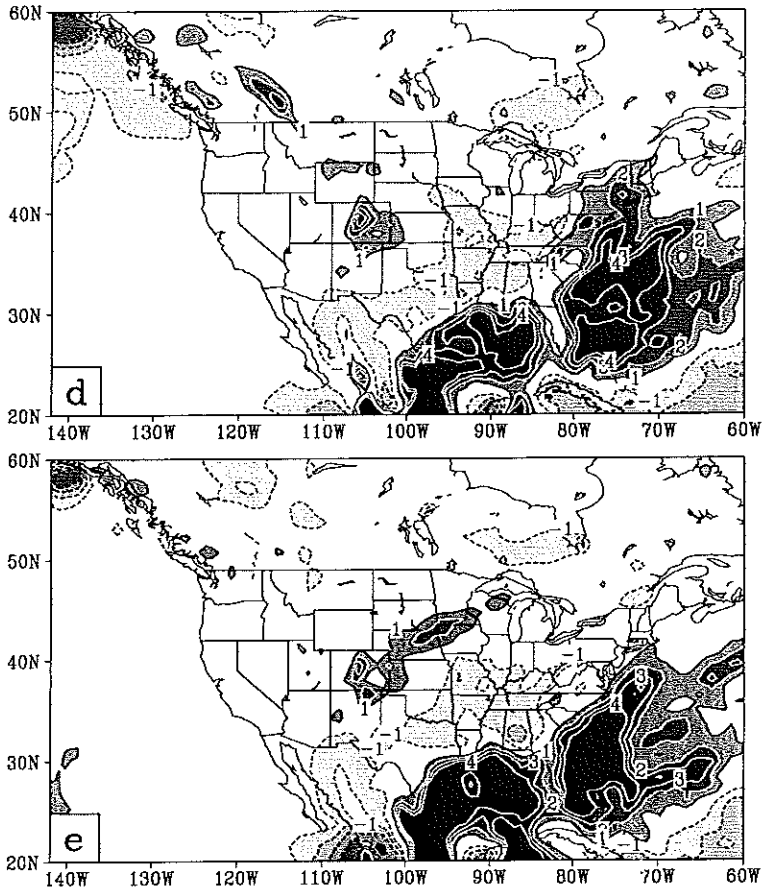

Fig. 4 (continued)

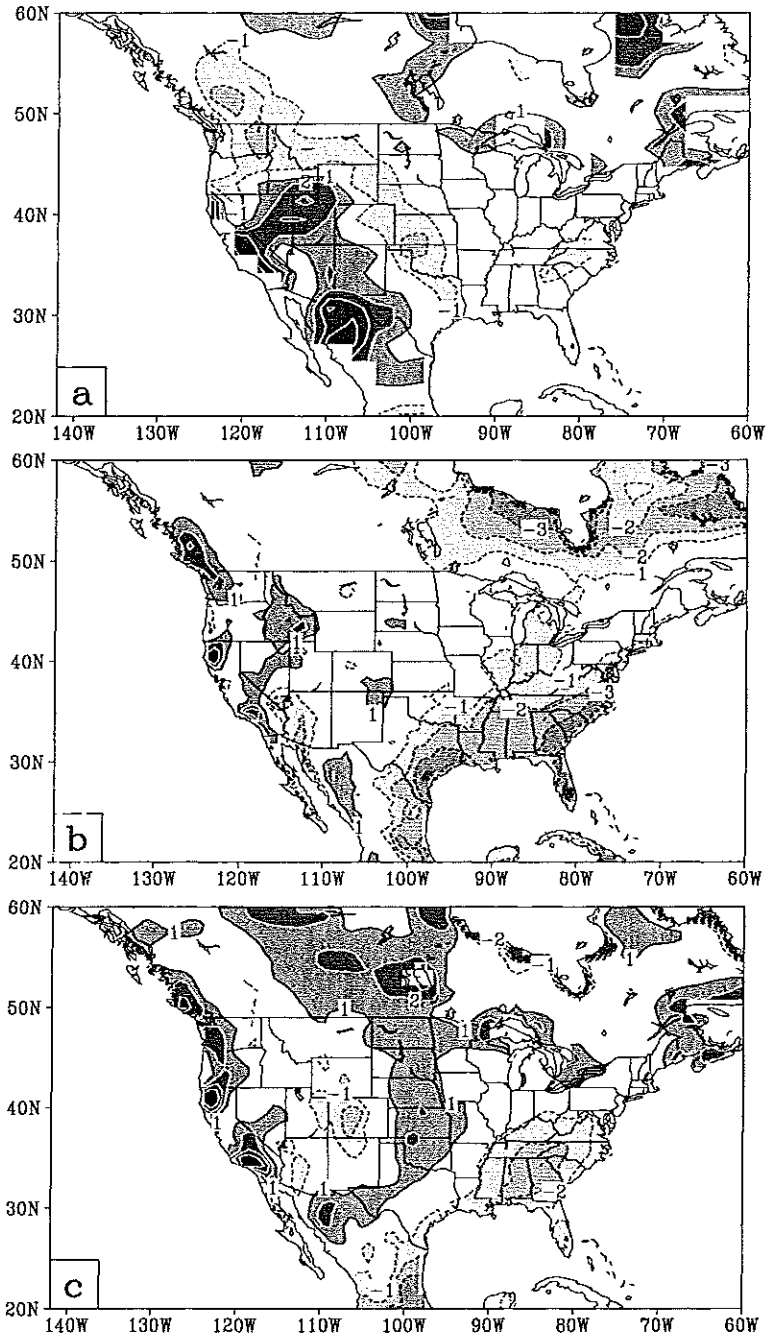

Fig. 5. JJAS 3-year mean surface temperature error for a) COLA GCM, b) Eta, c) RSM, d) MM5V3 and e) MM5V2. Contour interval is 1 °C with the zero contour omitted. In the COLA GCM, Eta and RSM, surface temperature is taken to be the calculated 2-meter shelter temperature, while in MM5 it is approximated by the temperature in the lowest model sigma layer. See text for a description of the observations and the method used to calculate the temperature errors.

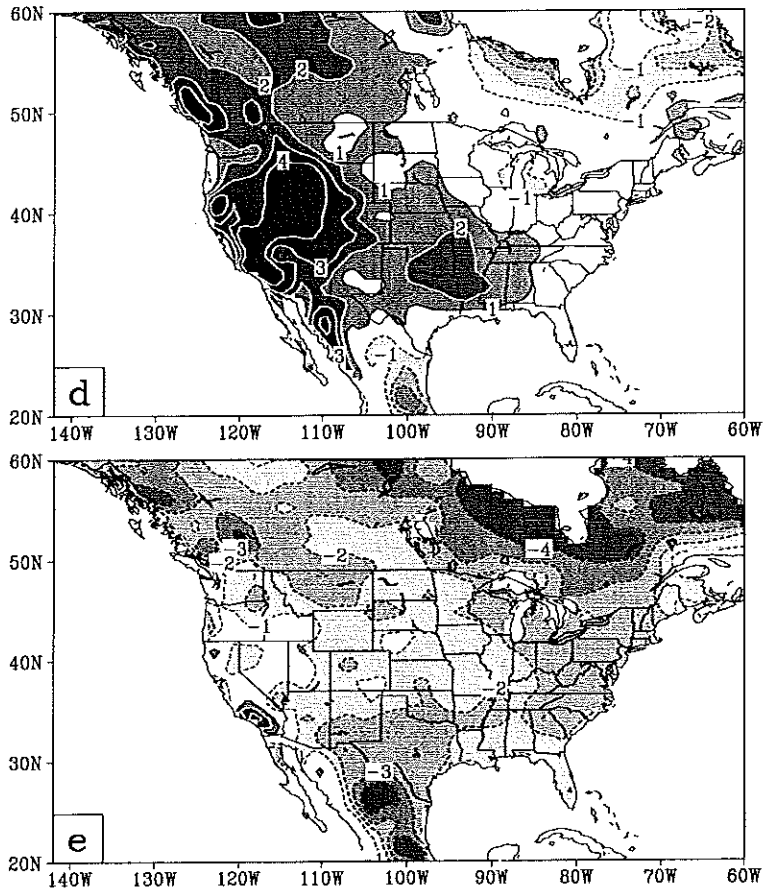

Fig. 5 (continued)

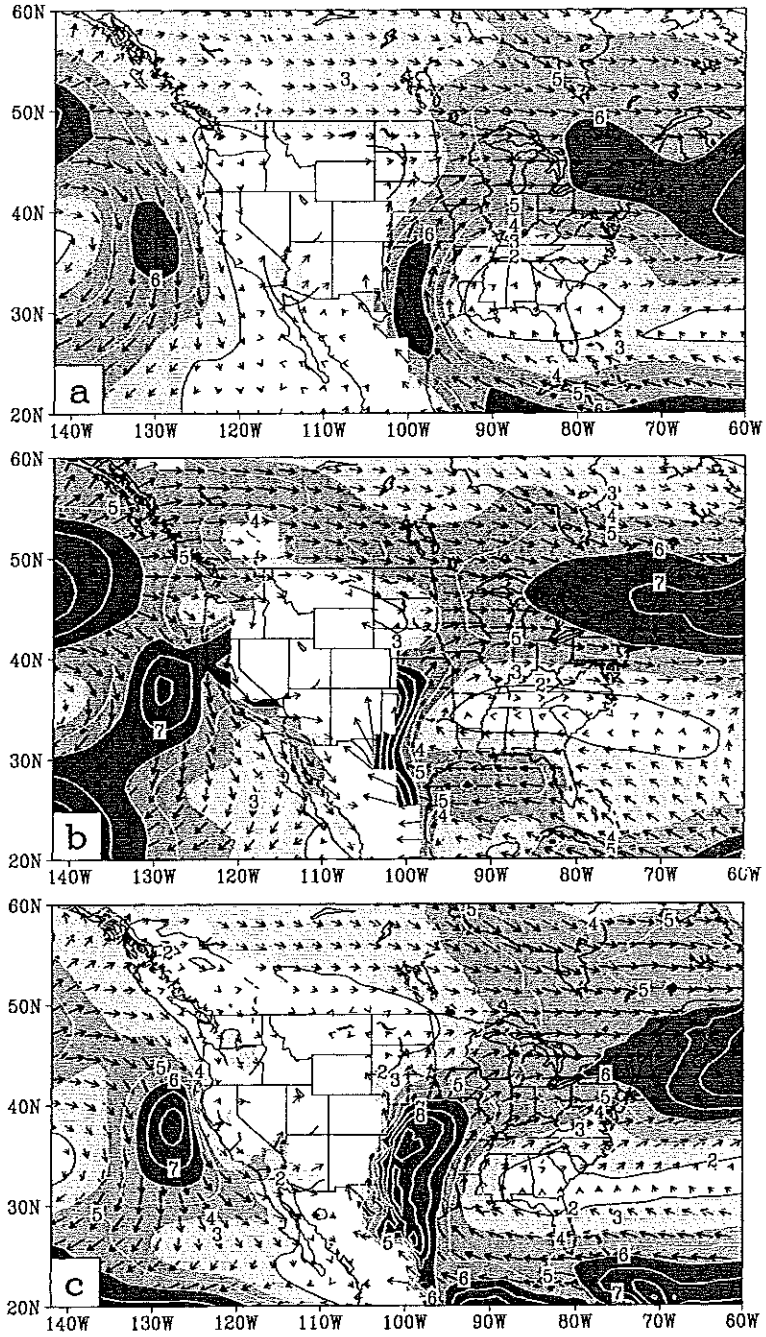

Fig. 6. JJAS 3-year mean 850-mb wind vectors and isotachs for a) NCEP/NCAR reanalysis, b) COLA GCM, c) Eta, d) RSM, e) MM5V3 and f) MM5V2. Contour interval is 1 m s^{-1} with the 1 m s^{-1} contour omitted.

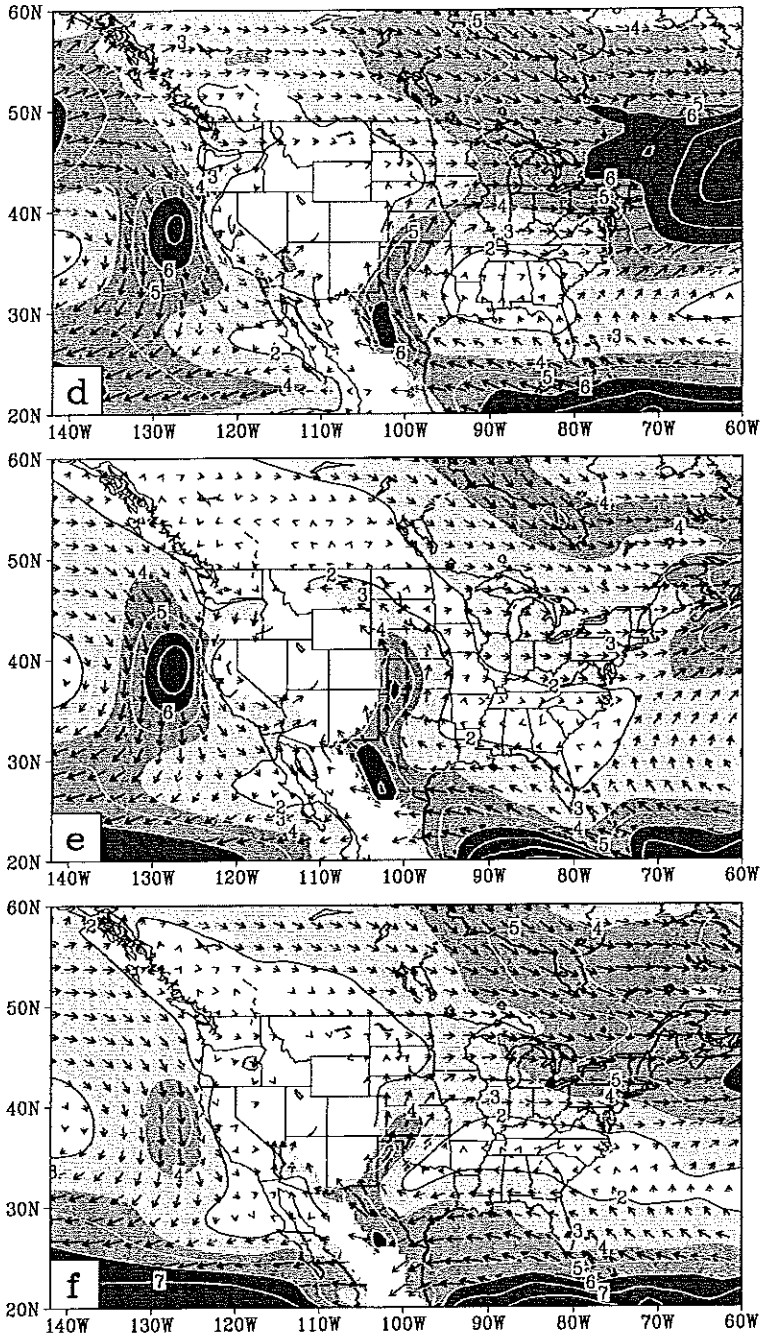

Fig. 6 (continued)

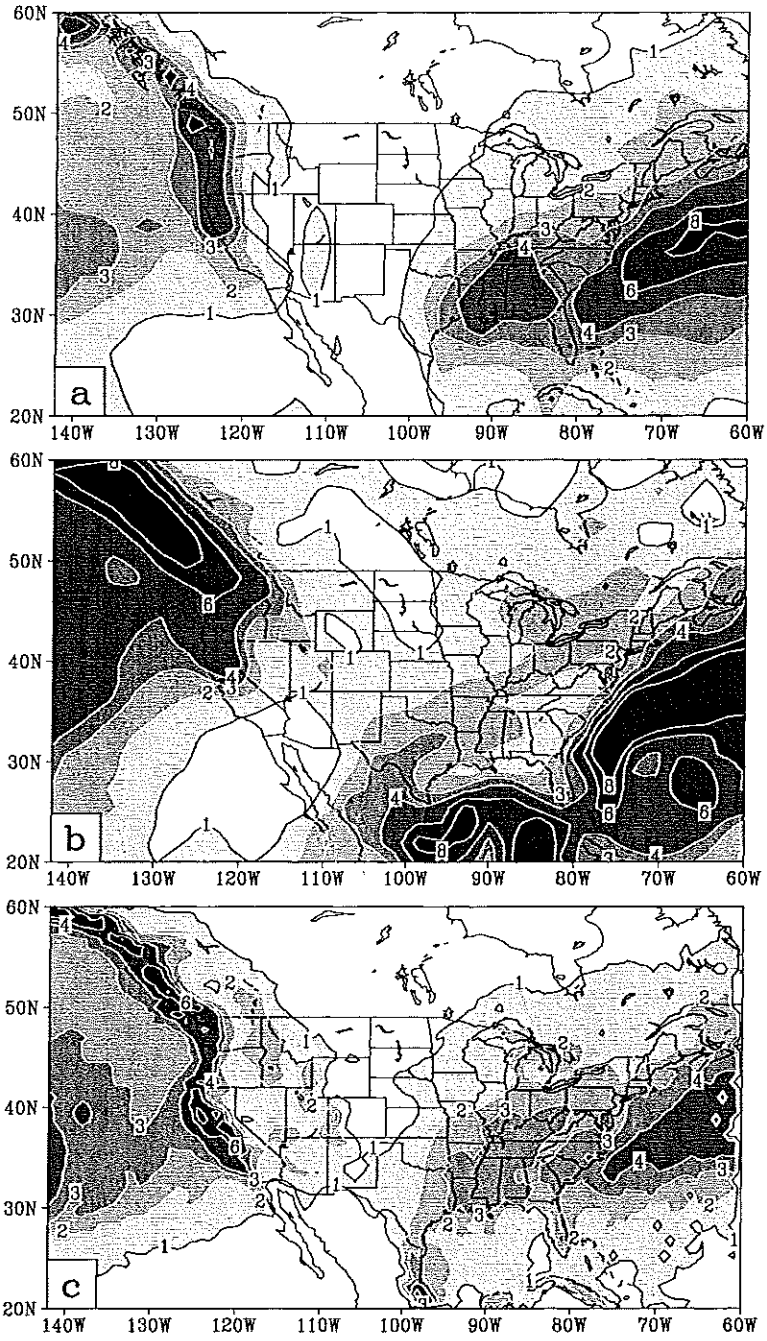

Fig. 7. JFM 3-year mean precipitation for a) Xie-Arkin observations, b) COLA GCM, c) Eta, d) RSM, e) MM5V3 and f) MM5V2. Contours are 1, 2, 3, 4, 6, 8 mm d^{-1}.

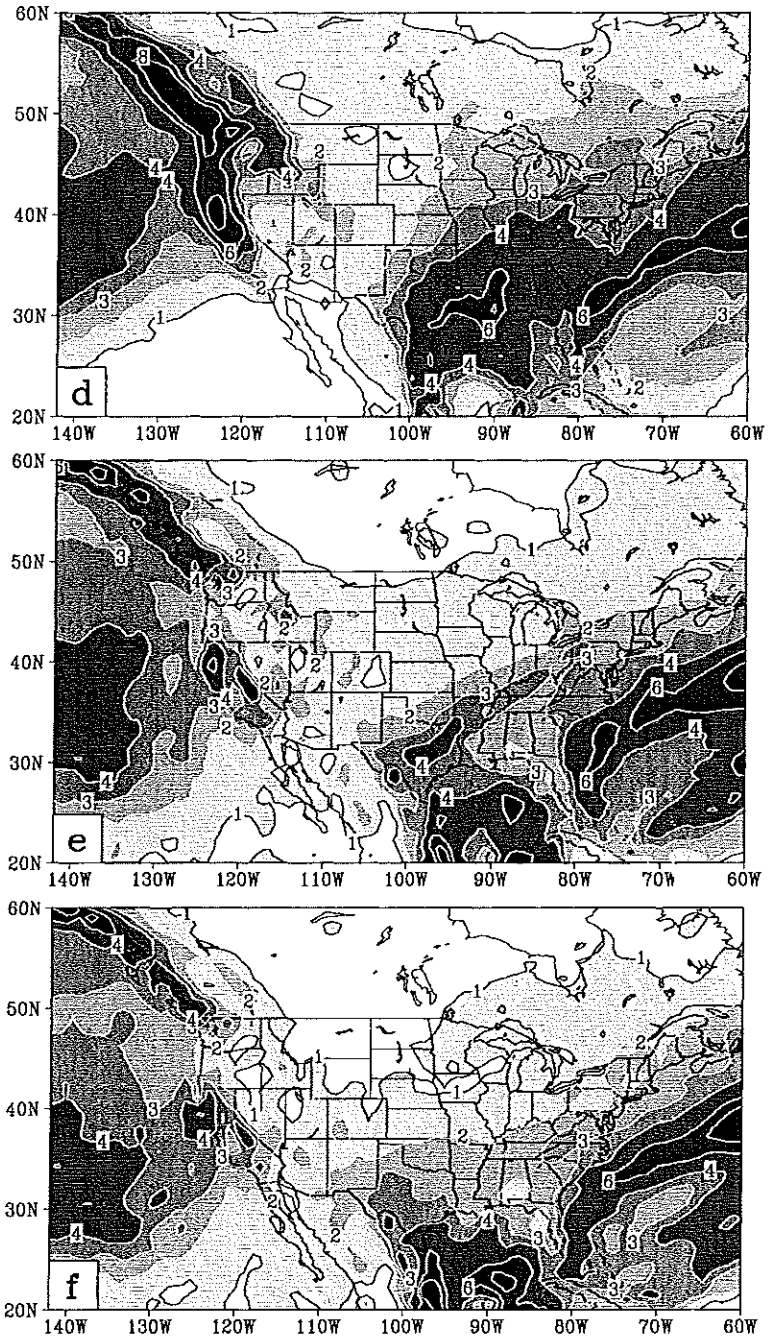

Fig. 7 (continued)

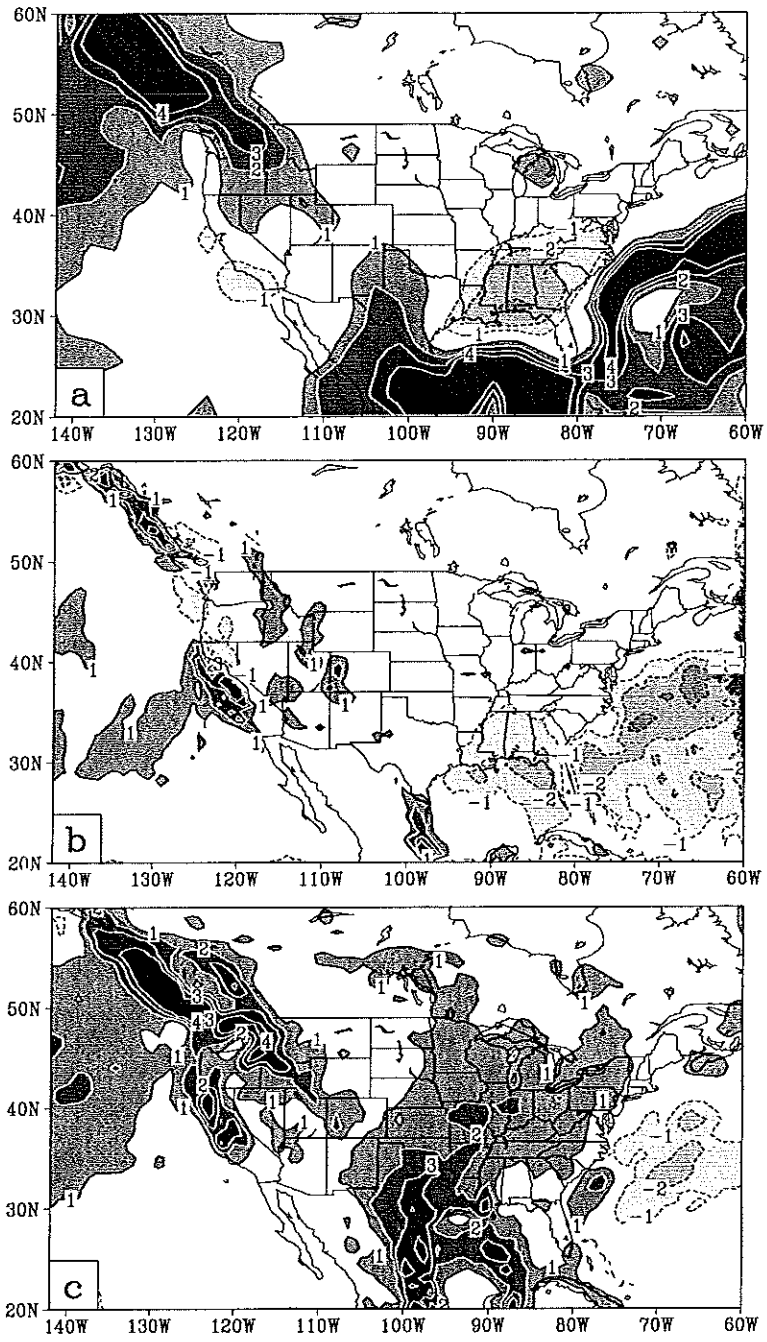

Fig. 8. JFM 3-year mean precipitation error for a) COLA GCM, b) Eta, c) RSM, d) MM5V3 and e) MM5V2. Contours are ±1, 2, 3, 4 mm d^{-1}.

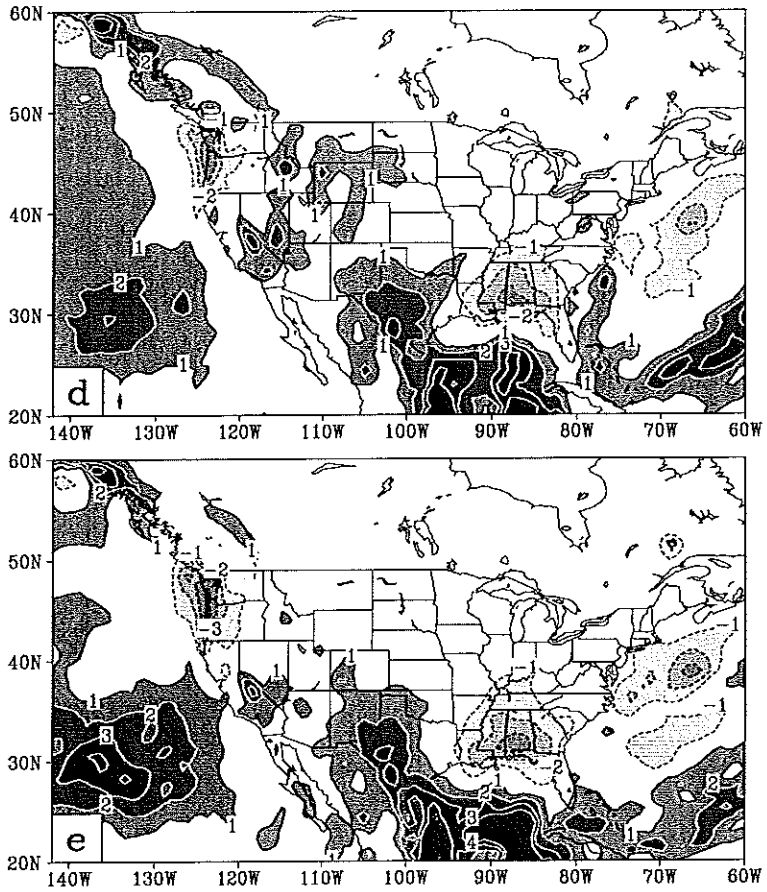

Fig. 8 (continued)

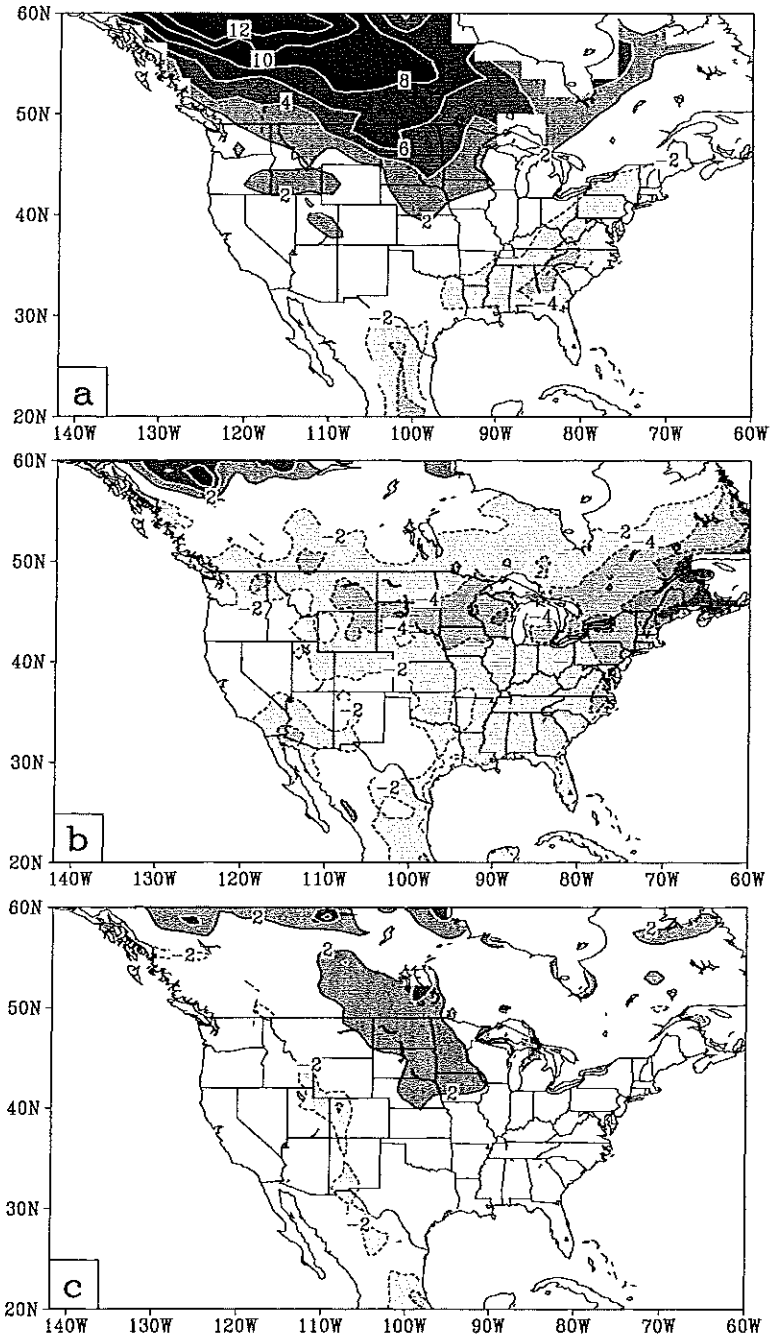

Fig. 9. JFM 3-year mean surface temperature error for a) COLA GCM, b) Eta, c) RSM, d) MM5V3 and e) MM5V2. Contour interval is 2°C with the zero contour omitted.

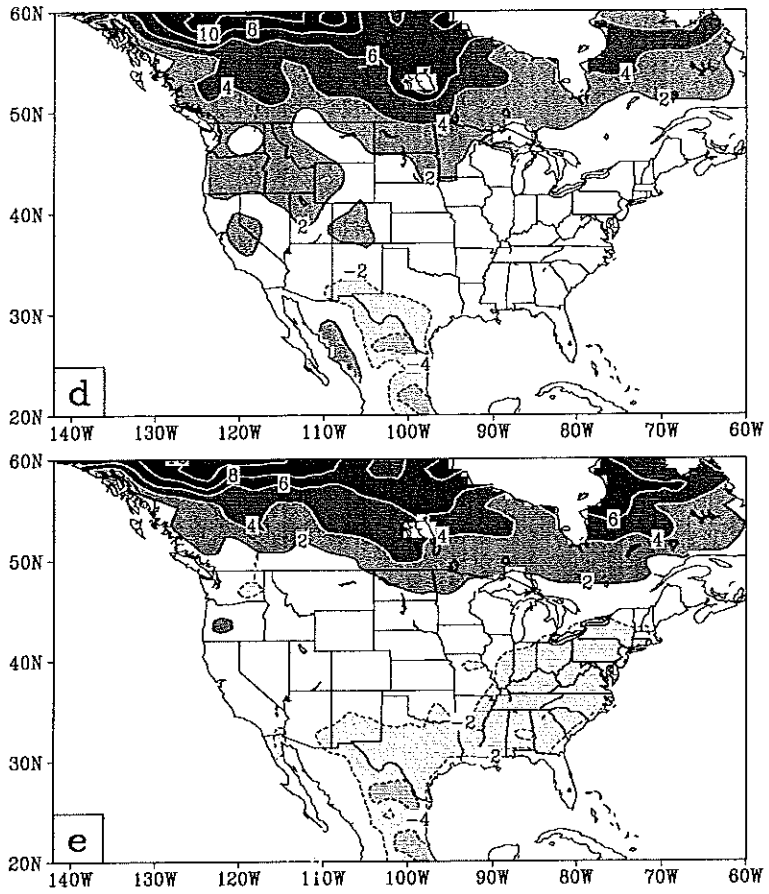

Fig. 9 (continued)

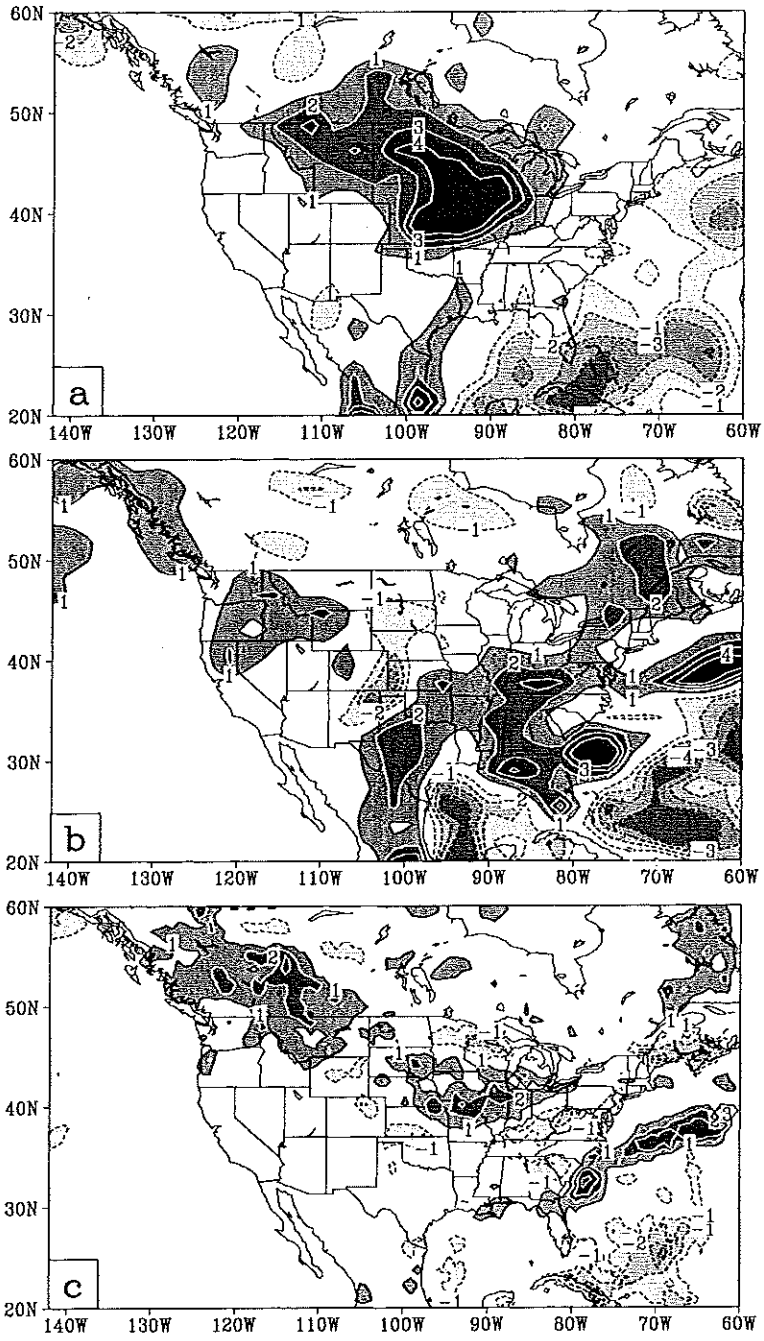

Fig. 10. June-July mean 1993 minus 1988 precipitation difference for a) Xie-Arkin observations, b) COLA GCM, c) Eta, d) RSM, e) MM5V3 and f) MM5V2. Contours are ±1, 2, 3, 4 mm d^{-1}.

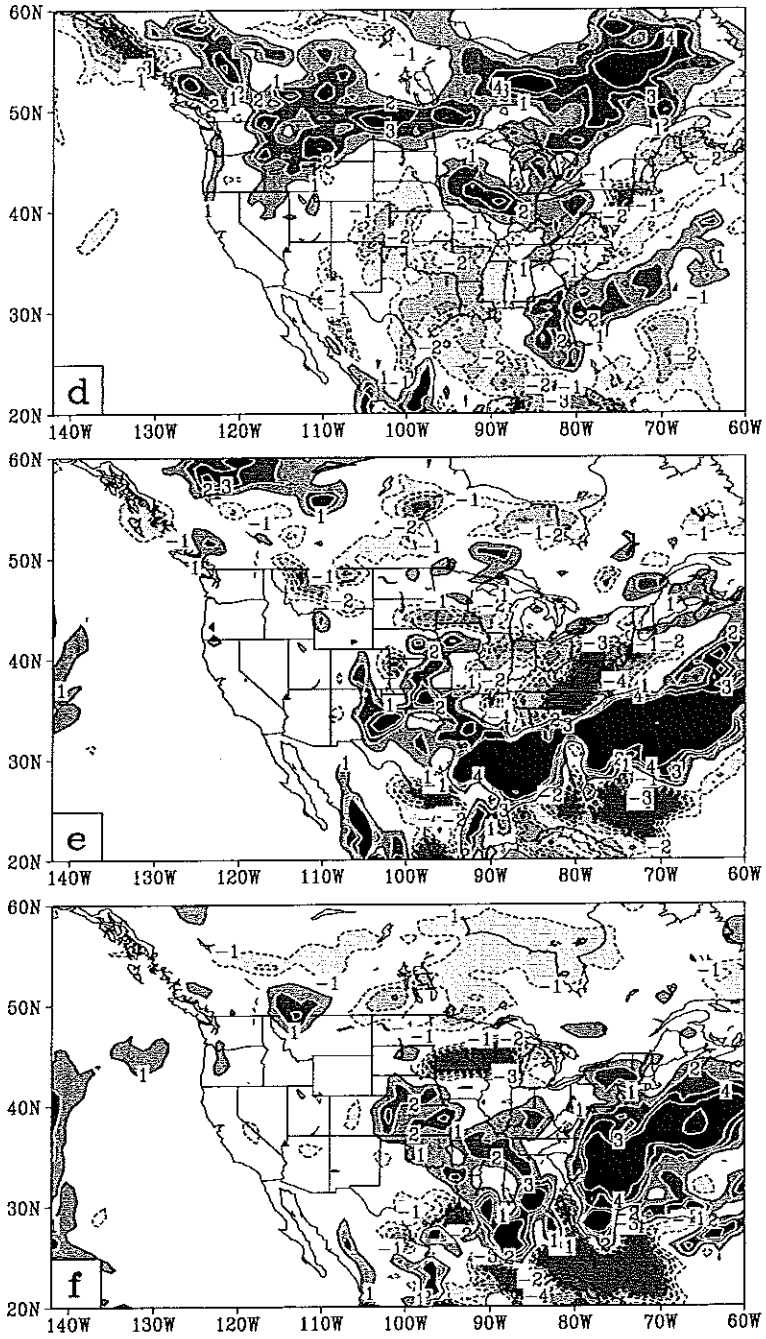

Fig. 10 (continued)

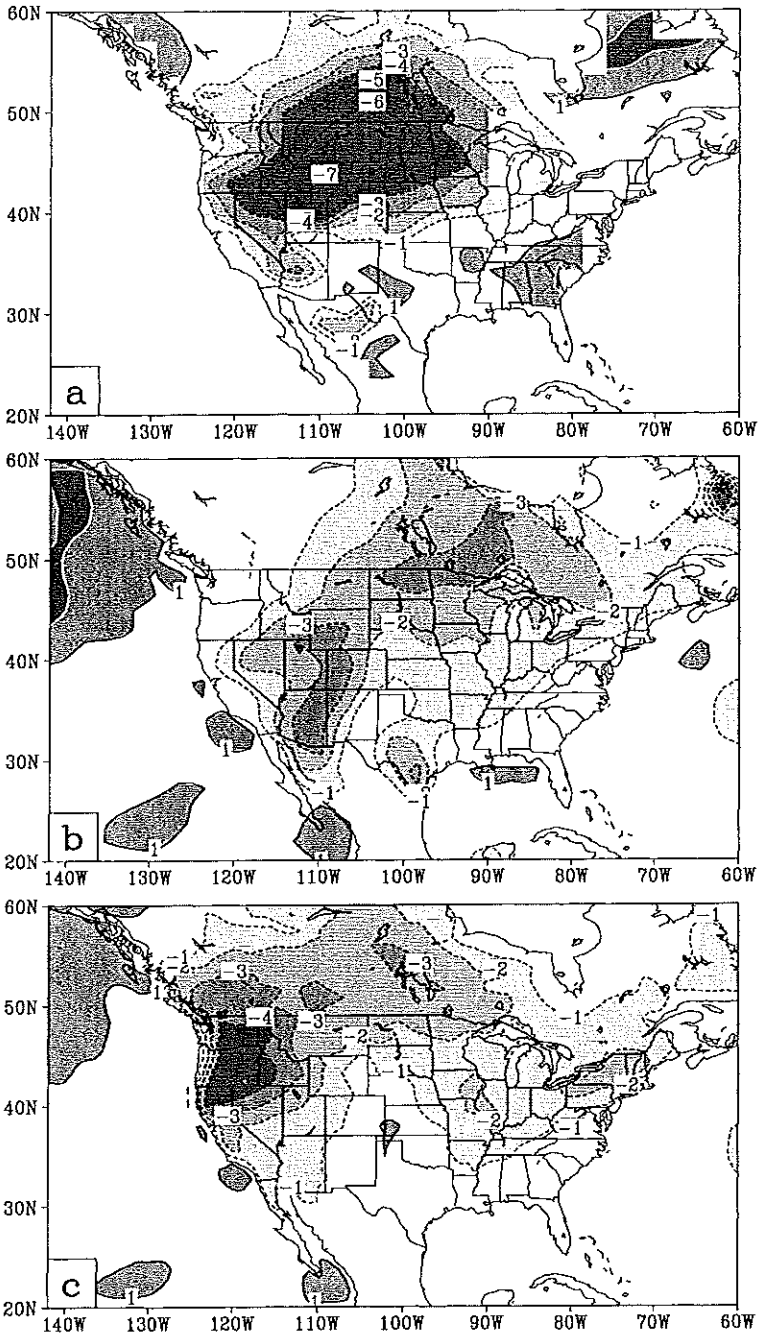

Fig. 11. June-July mean 1993 minus 1988 surface temperature difference for a) observations (see text), b) COLA GCM, c) Eta, d) RSM, e) MM5V3 and f) MM5V2. Contour interval is 1 °C with the zero contour omitted.

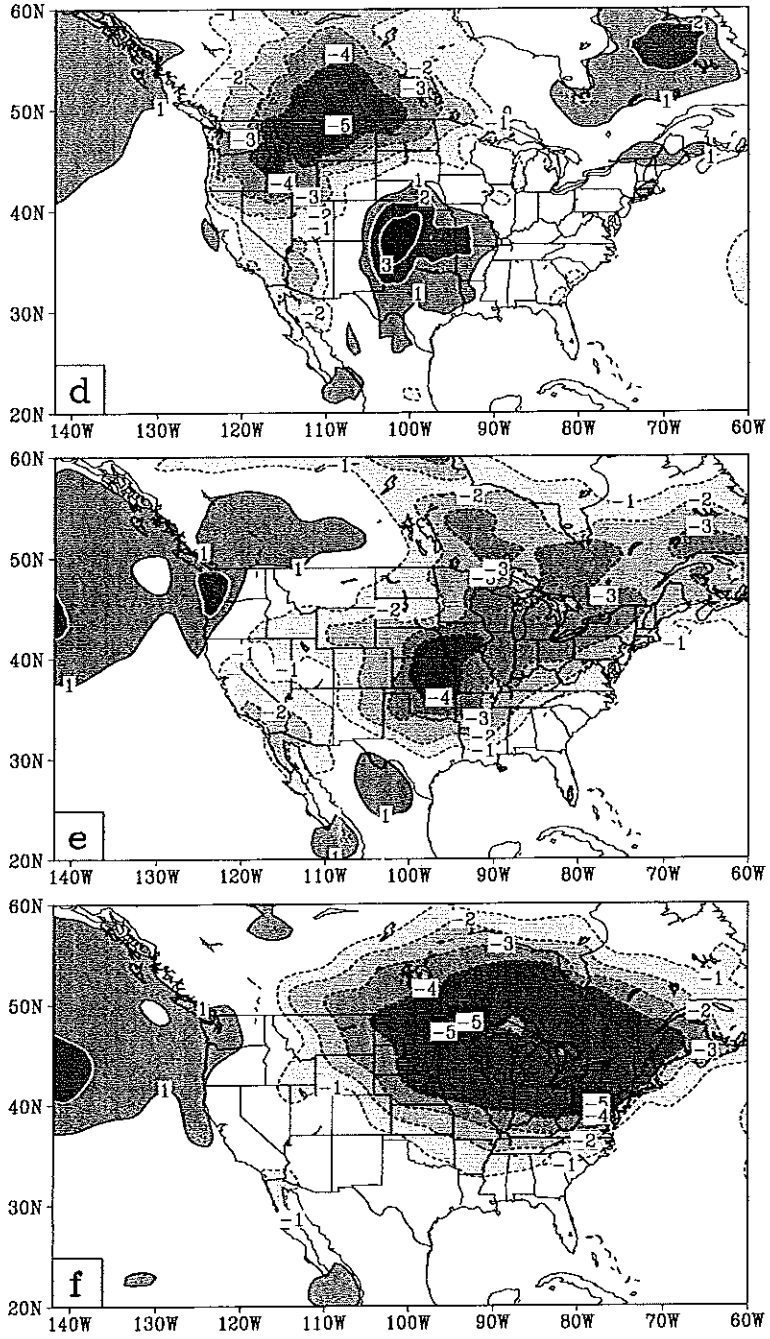

Fig. 11 (continued)

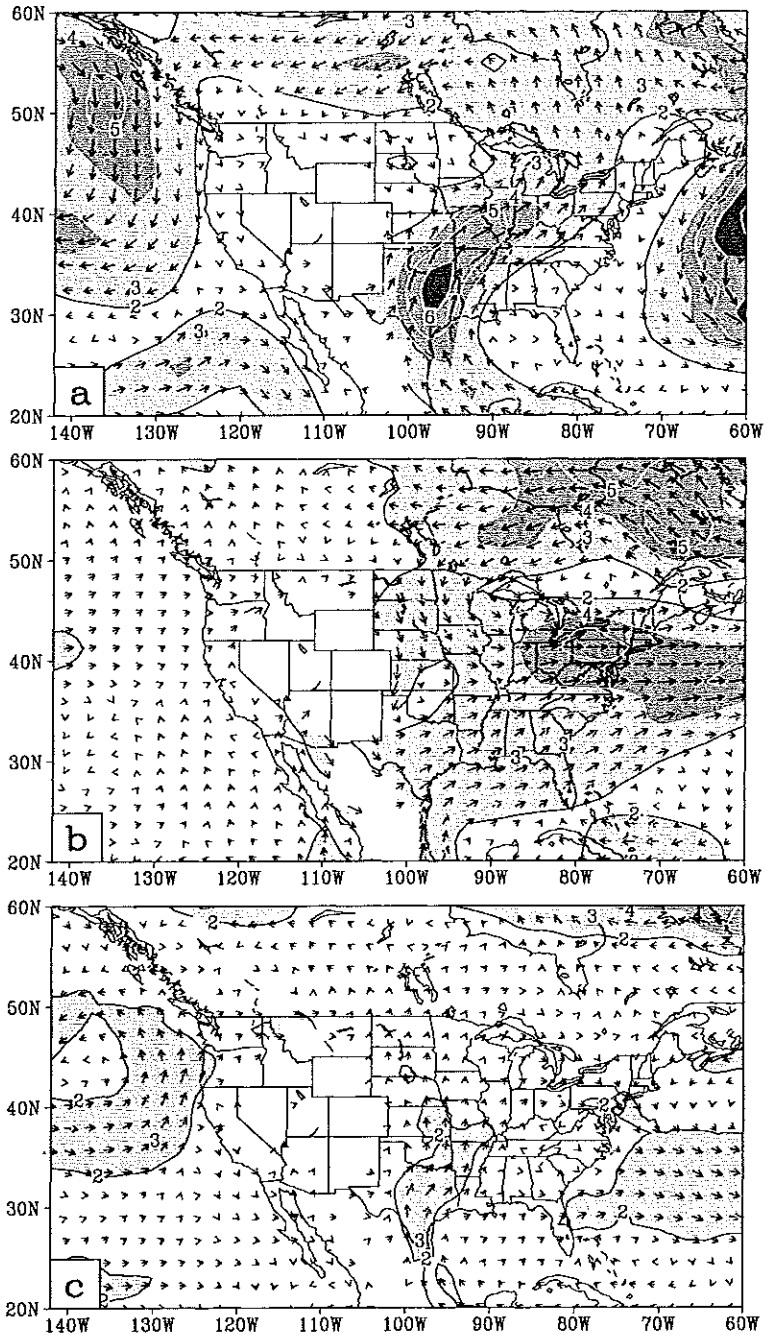

Fig. 12. June-July mean 1993 minus 1988 850-mb wind difference vectors and isotachs for a) NCEP/NCAR reanalysis, b) COLA GCM, c) Eta, d) RSM, e) MM5V3 and f) MM5V2. Contour interval is 1 m s^{-1} with the 1 m s^{-1} contour omitted.

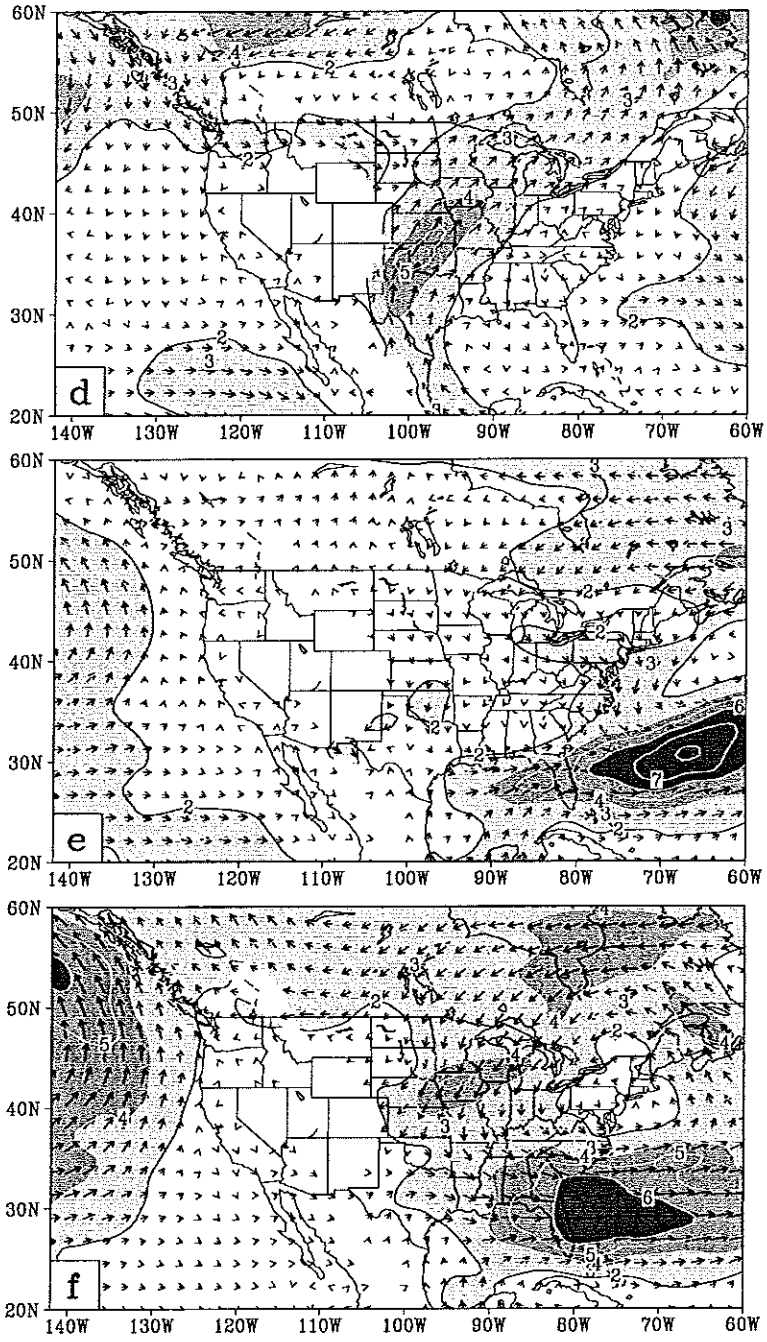

Fig. 12 (continued)

COLA Technical Reports

1 Ocean Wave Dynamics and El Niño. *E. K. Schneider, B. Huang, & J. Shukla*, April 1994, 46 pp.

2 Flux Correction and Equilibrium Climate. *E. K. Schneider*, April 1994, 12 pp.

3 The Effect on Climate of Doubling Deserts. *P. A. Dirmeyer, & J. Shukla*, June 1994, 61 pp.

4 A Comparison of Two Surface Wind Stress Analyses over the Tropical Atlantic during 1980-1987. *B. Huang, & J. Shukla*, June 1994, 46 pp.

5 A Pilot Reanalysis Project at COLA. *D. Paolino, Q. Yang, B. Doty, J. L. Kinter III, J. Shukla, & D. Straus*, July 1994, 46 pp.

6 GCM Simulations of the Life Cycles of the 1988 US Drought and Heatwave. *M. J. Fennessy, J. L. Kinter III, L. Marx, E. K. Schneider, P. J. Sellers, & J. Shukla*, July 1994, 68 pp.

7 Land-Sea Geometry and its Effect on Monsoon Circulations. *P. A. Dirmeyer*, August 1994, 39 pp.

8 The response of an Ocean GCM to Surface Wind Stress Produced by an Atmospheric *GCM. B. Huang, & E. K. Schneider*, September 1994, 56 pp.

9 Meeting on Problems in Initializing Soil Wetness: Review. *P. A. Dirmeyer*, January 1995, 33pp.

10 Experimental Multi-Season ENSO Predictions with an Anomaly Coupled General Circulation Model. *Z. Zhu and E. K. Schneider*, May 1995, 28pp.

11 The Impact of Desertification in the Mongolian and the Inner Mongolian Grassland on the East Asian Monsoon. *Yongkang Xue*, May 1995, 50pp.

12 Annual Cycle and ENSO in a Coupled Ocean-Atmosphere Model. *Edwin K. Schneider, Zhengxin Zhu, Benjamin S. Giese, Bohua Huang, Ben P. Kirtman, J. Shukla, James A. Carton*, May 1995, 57pp.

13 Improvement in Stratosphere and Upper-Troposphere Simulation with a Hybrid Isentropic-Sigma Coordinate GCM. *Zhengxin Zhu and Edwin K. Schneider*, June 1995, 45pp.

14 Factors Determining the Precipitation Distribution and Low-Level Flow in the Tropics of an Atmospheric General Circulation Model: Diagnostic Studies. *David G. DeWitt, Edwin K. Schneider, and Anandu D. Vernekar*, June 1995, 56pp.

15 Multiseasonal Predictions with a Coupled Tropical Ocean Global Atmosphere System. *Ben P. Kirtman, J. Shukla, Bohua Huang, Zhengxin Zhu, and Edwin K. Schneider*, June 1995, 59pp.

16 An Examination of the AGCM Simulated Surface Wind Stress and Low Level Winds Over the Tropical Pacific Ocean. *Bohua Huang and J. Shukla*, August 1995, 42pp.

17 Model Based Estimates of Equatorial Pacific Wind Stress. *Ben P. Kirtman, Edwin K. Schneider and Bernard Kirtman*, August 1995, 58pp.

18 Impact of Vegetation Properties on U.S. Summer Weather Prediction. *Yongkang Xue, Michael J. Fennessy and Piers Sellers*,August 1995, 41pp.

19 Wave-CISK, The Evaporation-Wind Feedback, and the Intraseasonal Oscillation: Phase Propagation and Scale Selection. *Ben P. Kirtman and Anandu D. Vernekar*,August 1995.

20 Intercomparison of Atmospheric Model Wind Stress with Three Different Convective

Parameterizations: Sensitivity of Tropical Pacific Ocean Simulations. *Ben P. Kirtman and David G. DeWitt,* September 1995, 51 pp.

21 Variations of Mid-Latitude Transient Dynamics Associated with ENSO. *David M. Straus and J. Shukla,*September 1995, 49 pp.

22 Tropical Influence on Global Climate. *Edwin K. Schneider, Richard S. Lindzen and Ben P. Kirtman,* February 1996, 29pp.

23 Precipitation and Water Vapor Transport Simulated by a Hybrid Isentropic-Sigma GCM. *Zhengxin Zhu,*March 1996, 37 pp.

24 Predictability and Error Growth in a Coupled Ocean-Atmosphere Model. *J. Shukla and Ben P. Kirtman,* March 1996, 11 pp.

25 Diagnosis of the Mid-Latitude Baroclinic Regime in the NASA DAO Reanalyses and ECMWF Operation Analyses *David M. Straus and Dan Paolino,* March 1996, 48 pp.

26 Proceedings of the Workshop on Dynamics and Statistics of Secular Climate Variations: Miramare - Trieste, Italy; 4 - 8 December 1995 Editors: *James L. Kinter III and Edwin K. Schneider,* April 1996.

27 The Effect of Cumulus Convection on the Climate of the COLA General Circulation Model, *David DeWitt,* May 1996, 58pp.

28 Oceanic Rossby Waves and the ENSO Period in a Coupled Model , *Ben P. Kirtman,* May 1996, 49 pp.

29 Biosphere Feedback on Regional Climate in Tropical North Africa, *Yongkang Xue,* June 1996.

30 Characteristics of the Interannual and Decadal Variability in a General Circulation Model, *Bohua Huang and J. Shukla,* July 1996, 55pp.

31 Scale Dependent Forcings of a General Circulation Model, *David Straus and Yuhong Yi,* July 1996, 34pp.

32 ENSO Simulation and Prediction with a Hybrid Coupled Model, *Ben P. Kirtman and Stephen E. Zebiak,* August 1996, 50pp.

33 Seasonal Atmospheric Prediction, *Larry Marx and Michael J. Fennessy,* August 1996, 34pp.

34 Impact of Initial Soil Wetness on Seasonal Atmospheric Prediction, *Michael J. Fennessy and J. Shukla,* August 1996, 37pp.

35 The Earth Radiation Budget as Simulated by the COLA GCM, *David G. DeWitt and Edwin K. Schneider,* November 1996, 39pp.

36 A Note on the Annual Cycle of Sea Surface Temperature at the Equator, *Edwin K. Schneider,* December 1996, 16pp.

37 Sensitivity of the Simulated Annual Cycle of Sea Surface Temperature in the Equatorial Pacific to Sunlight Penetration. *Edwin K. Schneider and Zhengxin Zhu,* March 1997, 37pp.

38 A Global Ocean Data Analysis for 1986-1992. *Bohua Huang and James L. Kinter III,* March 1997, 62pp.

39 ENSO Hindcasts with a Coupled GCM. *Edwin Schneider, Zhengxin Zhu, David DeWitt, Bohua Huang, and Ben Kirtman,* April 1997, 40pp.

40 GCM Simulations of Intraseasonal Variability in the Indian Summer Monsoon. *R. Krishnan and M.J. Fennessy,* April 1997, 54pp.

41 Model Simulation of the Influence of Global SST Anomalies on the Sahel Rainfall. *Yongkang Xue and Jagadish Shukla*, April 1997, 25pp.

42 Predicting Wintertime Skill from Ensemble Characteristics in the NCEP Medium Range Forecasts over North America. *Paul A. Dirmeyer, Brian E. Doty and James L. Kinter III*, April 1997, 31pp.

43 Decadal Variability in ENSO Predictability and Prediction. *Ben P. Kirtman and Paul S. Schopf*, May 1997, 43pp.

44 Simulations of the Climate with a Coupled Ocean-Atmosphere General Circulation Model: Seasonal Cycle and Adjustment to Mean Climate. *David G. DeWitt and Edwin K. Schneider*, July 1997, 64pp.

45 Upper Tropospheric Water Vapor and Climate Sensitivity. *Edwin K. Schneider, Ben P. Kirtman and Richard S. Lindzen*, August 1997, 40pp.

46 A Broad Scale Circulation Index for the Interannual Variability of the Indian Summer Monsoon. *B.N. Goswami, V. Krishnamurthy, and H. Annamalai*, September 1997, 52pp.

47 Assessing GCM Sensitivity to Soil Wetness Using GSWP Data, *Paul A. Dirmeyer*, September 1997, 26pp.

48 A Two Dimensional Implementation of the Simple Biosphere (SiB) Model, *Paul A. Dirmeyer and Fanrong Zeng*, September 1997, 30pp.

49 Using SST Anomalies to Predict Flood and Drought Conditions for the Caribbean, *A. Chen, A. Roy, J. McTavish, M. Taylor and L. Marx*, September 1997, 41pp.

50 A Forecast of Precipitation and Surface Air Temperature in North America for Winter (JFM) 1998, *J. Shukla, Dan Paolino, Ben Kirtman, David DeWitt, Paul Dirmeyer, Brian Doty, Mike Fennessy, Bohua Huang, James Kinter, Larry Marx, Edwin Schneider, David Straus, Z. Zhu*, September 1997, 14pp.

51 The COLA Atmosphere-Biosphere General Circulation Model Volume 1: Formulation, *James L. Kinter III, David DeWitt, Paul A. Dirmeyer, Michael J. Fennessy, Ben P. Kirtman, Larry Marx, Edwin K. Schneider, J. Shukla and David Straus*, October 1997, 46pp.

52 Climatology and Interannual Variability of Northern Hemisphere Snow Cover and Depth Based on Satellite Observations, *A.S. Bamzai and J.L. Kinter III*, November 1997, 48pp.

53 Relation Between Eurasian Snow Cover, Snow Depth and the Indian Summer Monsoon: An Observational Study, *A. Bamzai and J. Shukla*, February 1998, 42pp.

54 Influence of the Indian Summer Monsoon on ENSO, *B. Kirtman and J. Shukla* , May 1998, 52pp.

55 A Fundamental Limitation of Markov Models, *T. DelSole*, May 1998, 32pp.

56 The Tropical Ocean Response to a Change in Orbital Forcing, *D. DeWitt and E.K. Schneider*, July 1998, 55pp.

57 Modeling the Effects of Vegetation on Mediterranean Climate During the Roman Classical Period Part I: Climate History and Model Sensitivity, *O. Reale and P. Dirmeyer*, August 1998, 47pp.

58 Modeling the Effects of Vegetation on Mediterranean Climate During the Roman Classical Period Part II: Climate History and Model Simulation, *O. Reale and J. Shukla*, August 1998, 68pp.

59 A Dissipation Integral with Application to Ocean Diffusivities and Structure, *E. Schneider and U. Bhatt*, September 1998, 37pp.

60 Geophysical Turbulence in the Reanalyses of ECMWF , *D. Straus and P. Ditlevsen*, October 1998, 50pp.

61 Simulations of a Boreal Grassland Hydrology at Valdai, Russia: PILPS Phase 2(d) , *C. A. Schlosser and Collaborators*, October 1998, 47pp.

62 Monsoon-ENSO Relationship on Interdecadal Time Scale , *V. Krishnamurthy and B.N. Goswami*, October 1998, 55pp.

63 Seasonal Prediction Experiments with a Regional Model Nested in a Global Model, *M.J. Fennessy and J. Shukla*, December, 1998, 47pp.

64 A Spontaneously Generated Atmospheric General Circulation, *Ben P. Kirtman and Edwin K. Schneider*, March, 1999, 37pp.

65 GCM Simulation of the relationship between spring Eurasian snow and Indian summer monsoon, *A.S. Bamzai and L. Marx*, March, 1999, 30pp.

66 Distinguishing Between the SST-forced Variability and Internal Variability in Mid-Latitudes: Analysis of Observations and GCM Simulations, *David M. Straus and J. Shukla,* April, 1999, 54pp.

67 Dynamical Seasonal Predictions with the COLA Atmospheric Model, *J. Shukla, D.A. Paolino, D.M. Straus, D. DeWitt, M. Fennessy, J.L. Kinter, L. Marx, R. Mo,* May,1999, 42pp.

68 Using a Global Soil Wetness Data Set to Improve Seasonal Climate Simulation, *Paul A. Dirmeyer,* May, 1999, 42pp.

69 Intraseasonal and Interannual Variability of Rainfall over India, *V. Krishnamurthy and J. Shukla,* August, 1999, 34pp, in press.

70 A Model for Transient Eddy Momentum Fluxes in the Upper Troposphere, *Timothy DelSole,* September, 1999, 38pp.

71 Optimally Persistent Patterns in Time-Varying Fields, *Timothy DelSole,* October, 1999, 46pp.

72 An Ocean Data Assimilation System with Intermittent Analyses and Continuous Model Error Correction, *Bohua Huang, James L. Kinter III, Paul S. Schopf* , October, 1999, 60pp.

73 Statistical Verification of Dynamical Seasonal Prediction, *Ruping Mo and David M. Straus,* November, 1999, 73pp.

74 Probability Forecasts for Seasonal Average Anomalies Based on GCM Ensemble Means, *Ruping Mo and David M. Straus,* November, 1999, 33pp.

75 Seasonal Prediction Based on EOF Analyses of GCM Ensemble Means, *Ruping Mo and David M. Straus,* November, 1999, 37pp.

76 An Approach for Quantifying Inter-model Variability, *C. Adam Schlosser and Tim DelSole,* November, 1999, 15pp.

77 Empirically Reducing the Systematic Error of an OGCM, *Ben P. Kirtman,* December, 1999, 40pp.

78 An update to the distribution and treatment of vegetation and soil properties in SSiB, *Paul A. Dirmeyer and Fanrong J. Zeng,* December, 1999, 37pp.

79 Application of a Precipitation Downscaling Model to Gridded Multi-sensor Radar Analyses, *Venugopal V. and P.A. Dirmeyer,* February, 2000, 25pp.

80 Impact of Tropical Subseasonal SST Variability on Seasonal Mean Climate Simulations, *Ben P. Kirtman, Dan A. Paolino, James L. Kinter III and David M. Straus*, Feburary, 2000, 40pp.

81 Observed and Model Simulated Interannual Variability of the Indian Monsoon, *V. Krishnamurthy and J. Shukla,* May, 2000, 46pp.

82 Climate drift in a coupled land-atmosphere model, *Paul A. Dirmeyer,* July, 2000, 21pp

83 Modeling the Effects of the Andes on the South American Climate, *Clemente A.S. Tanajura and Jagadish Shukla,* August, 49pp.

84 A Stochastic Similarity Hypothesis for Large-Scale Turbulence, *Timothy DelSole, August, 2000,* 37pp.

85 Regional Simulation of Interannual Variability over South America, *Vasubandhu Misra, Paul A. Dirmeyer, Ben P. Kirtman, Hann-Ming Henry Juang and Masao Kanamitsu,* August 2000, 42pp.

86 The Indonesian Throughflow's Effect on Global Climate Determined from the COLA Coupled Climate System, *Roxana C. Wajsowicz and Edwin K. Schneider, September, 2000, 26pp.*

87 Experimental ENSO Predictions with a CGCM· A comparison of Two Different Approaches, *Zhengxin Zhu, Edwin K. Schneider, and Bohua Huang, September, 2000, 39pp.*

88 Evaporative moisture sources during a sequence of floods in the Mediterranean region, *Oreste Reale, Laura Feudale and Barbara Turato, September 2000, 15pp.*

89 An Evaluation of the Strength of Land-Atmosphere Coupling, *Paul A. Dirmeyer, October, 2000,* 34pp.

90 Analysis of the Connection from the South Asian Monsoon to ENSO by Using Precipitation and Circulation Indices, K. Miyakoda, J. Kinter and S. Yang, in press.

91 Climate Variability and Potential Predictability over Continental Regions in Response to SST Variations, *C. Adam Schlosser and Paul A. Dirmeyer,* October, 2000, 42pp.

92 A 36-Year Climatology of the Evaporative Sources of Warm-Season Precipitation oin the Mississippi River Basin, *Kaye L. Brubaker, Paul A. Dirmeyer, Arief Sudradjat, Benjamin S. Levy, and Fredric Bernal,* November, 2000, 48pp

93 New Astronomy in the COLA Atmospheric General Circulation Model, *L. Marx,* January,2001, 27pp.

94 The Interannual Variability in the Tropical Indian Ocean and its Relations to El Niño/Southern Oscillation, *Bohua Huang and James L. Kinter III,* January, 2001, 48pp

95 The Implementation of Simplified Simple Biosphere (SSiB) Scheme in the Regional Spectral Model (RSM), *Vasubandhu Misra, Paul A. Dirmeyer, and Ben P. Kirtman,* April, 2001, 31pp

96 Modeling the effect of land-surface variability on precipitation variability; Part I: General Response, *Oreste Reale and Paul A. Dirmeyer,* April, 2001, 33pp.

97 Modeling the effect of land-surface variability on precipitation variability, Part II: Spatial and time-scale structure, *Oreste Reale, Paul A. Dirmeyer and Adam Schlosser,* April, 2001, 39pp.

98 Understanding Differences Between the Equatorial Pacific as Simulated by Two Coupled GCMs, *Edwin K. Schneider,* May, 2001, 52pp

99 Does ENSO Force the PNA?, *David M. Straus and J. Shukla,* May, 2001, 39pp.

100 Near surface boreal summer climate as simulated by three general circulation models, *Paul A. Dirmeyer, Michael J. Fennessy, L. Marx*, June, 2001, 36pp.

101 Dynamic Downscaling of Seasonal Simulations Over South America, *Vasubandhu Misra, Paul A. Dirmeyer, and Ben P. Kirtman,* August, 2001, 28pp.

102 A Multi-Decadal Global Land-Surface Data Set of State Variables and Fluxes, *Paul A. Dirmeyer, Liqin Tan,* August, 2001, 43pp.

103 The COLA Global Coupled and Anomaly coupled Ocean-Atmosphere GCM, *Ben P. Kirtman, Yun Fan and Edwin K, Schneider*, August, 2001, 47pp.

104 A Shallow-CISK-Deep-Equilibrium Mechanism for the Interaction between Large-Scale Convection and Large-Scale Circulation in the Tropics, *Zhaohua Wu*, September, 2001, 40pp.

105 Interactive Coupled Ensemble: A new Coupling Strategy for CGCMs, *Ben P. Kirtman and J. Shukla*, September, 2001, 24pp.

106 A Model-Based Investigation of Soil-Moisture Predictability and Associated Climate Predictability, *C. Adam Schlosser and P.C.D. Milly*, September, 2001, 51pp.

107 Variability of the Indian Ocean: Relation to Monsoon and ENSO, *V. Krishnamurthy and Ben P. Kirtman,* September, 2001, 40pp.

108 A Simulation of the Tropical South American Summer Climate Variability with the NCEP ETA Model, *Anandu D. Vernekar, Ben P. Kirtman and Michael J. Fennessy*, October, 2001, 45pp.

109 Retrospective ENSO Forecasts: The Effect of Ocean Resolution, *Edwin K. Schneider, Ben P. Kirtman, Yun Fan, and Zengxin Zhu*, October, 2001, 27pp.

110 The Impact of Global Warming on ENSO Variability in Climate Records, *Zhaohua Wu, Edwin K. Schneider, Zeng-Zhen Hu, and Liqing Cao,* October, 2001, 22pp.

111 Entropy as a Basis for Comparing and Blending Forecasts, *Timothy DelSole*, December, 2001, 51pp.

112 Influence of North American Land Processes on North Atlantic SST Variability, *Uma S. Bhatt, Edwin K. Schneider & David DeWitt*, February 2002, 50pp.

113 The Role of ENSO in the South Asian Monsoon and Pre-Monsoon Signals Over the Tibetan Plateau, *K. Miyakoda, J.L. Kinter and Song Yang,* February, 2002, 44pp.

114 Linear Prediction of Indian Monsoon Rainfall, *Tim DelSole and J. Shukla,* March, 2002, 58pp.

Copies of COLA Reports are available from:

Center for Ocean-Land-Atmosphere Studies
4041 Powder Mill Road, Suite 302
Calverton, MD 20705-3106 USA